agriculture

MDPI

Article

Design and Performance Evaluation of a Self-Propelled Mugwort Harvester for Hilly and Mountainous Regions

Yi Li [1,*], Yongsheng He [1], Kai Zhang [1], Siqi Wang [1,2], Xinyu Hu [1] and Junnan Chen [1]

[1] School of Mechanical Engineering, Hubei University of Technology, Wuhan 430070, China; 102210123@hbut.edu.cn (Y.H.)
[2] School of Mechanical Engineering, Hubei Engineering University, Xiaogan 432000, China
* Correspondence: 20011013@hbut.edu.cn; Tel.: +86-153-4273-0330

Abstract: There are extensive areas of mugwort cultivation in China, making efficient harvesting crucial for the industry's economic performance. However, the lack of specialized harvesting machinery for hilly and mountainous regions leads to reliance on manual operations, characterized by high labor intensity and low efficiency. To address these issues, a self-propelled mugwort harvester is designed based on mugwort planting patterns and the physical characteristics of mugwort during the harvesting period. Key structural components, such as drum dimensions, tooth shapes, and tine arrangements, are developed, and a defoliation force model is established to identify factors influencing the net rate of mugwort leaf harvesting, impurity rate, and mugwort leaf usability. The harvester employs a fully hydraulic drive system, for which the hydraulic system is designed and components are selected. A quadratic regression orthogonal rotary test determines the optimal parameters: a forward speed of 0.8 m/s, drum speed of 200 r/min, and cutting table height of 50 mm. Field tests show that the harvester achieves a net rate of mugwort leaf harvesting of 93.78%, an impurity rate of 13.96%, a mugwort leaf usability of 86.23%, and an operational efficiency of 0.155 hm^2/h, while maintaining stable operation under field conditions. Beyond these performance metrics, the harvester reduces dependency on manual labor, lowers operational costs, and increases profitability for farmers. By improving the sustainability and mechanization of mugwort harvesting, this study provides an efficient solution for mugwort cultivation in hilly and mountainous regions and contributes to the sustainable development of the industry.

Keywords: *Artemisia argyi*; harvesting machine; cutting platform; tine drum; hydraulic transmission; orthogonal test

Academic Editor: Dainius Steponavičius

Received: 11 December 2024
Revised: 30 December 2024
Accepted: 3 January 2025
Published: 6 January 2025

Citation: Li, Y.; He, Y.; Zhang, K.; Wang, S.; Hu, X.; Chen, J. Design and Performance Evaluation of a Self-Propelled Mugwort Harvester for Hilly and Mountainous Regions. *Agriculture* **2025**, *15*, 111. https://doi.org/10.3390/agriculture15010111

1. Introduction

Mugwort (*Artemisia argyi*), a perennial herbaceous plant of the Asteraceae family, is widely cultivated across China due to its significant economic and medicinal value. Mugwort leaves are the primary ingredient in moxa sticks and moxa pillars, which are extensively used in moxibustion therapy for their efficacy in warming meridians, dispelling cold and dampness, and alleviating pain [1–5]. China is the largest producer and consumer of mugwort, with Hubei Province's Qichun region leading the industry, boasting a planting area of 15,618 hectares (ha) [6].

Despite the rapid growth in the mugwort industry, traditional harvesting methods remain predominantly manual. Farmers either use handheld mowing machines to cut the plants and manually strip the leaves in processing facilities, or directly strip the leaves by hand in the field. These methods are highly labor-intensive and time-consuming, making

them unsuitable for large-scale operations, leading to inefficiencies, high labor costs, and suboptimal yields. These challenges hinder the industry's modernization and sustainability. Mechanized harvesting methods, which can improve efficiency, reduce costs, and enhance productivity, have thus become increasingly urgently needed.

Mechanized mugwort harvesting has been the subject of extensive research. Domestic studies have made significant advancements in defoliation mechanisms and structural designs. Lai et al. [7] introduced a shear-strike hybrid defoliator that effectively mitigated leaf entanglement issues; however, its performance was constrained by difficulties in handling soft leaf tips. Sun [8] proposed a two-speed defoliation machine incorporating flexible tension spring components and parallel rollers, achieving enhanced efficiency and reduced impurity rates but catering primarily to dried mugwort. Wang [9] adopted a rotary blow defoliation principle with high-speed rotating drums to improve leaf detachment, yet its adaptability across mugwort varieties and working conditions remains constrained. Dong et al. [10] proposed a pneumatic bionic defoliation system simulating human hand movements, optimizing its parameters through orthogonal experiments, although concerns about its economic viability and durability persist. Zhou et al. [11] combined double-chain clamping with spiral defoliation rollers and stem-pulling mechanisms to improve the detachment of mugwort leaves from stems, achieving higher defoliation efficiency.

Despite these advancements, many existing designs are still limited to small-scale operations and lack adaptability to diverse terrains and environmental conditions. Furthermore, they often fail to meet the specific mechanical and operational demands of harvesting mugwort in challenging topographies.

This study develops a self-propelled mugwort harvester tailored for hilly and mountainous terrains, where conventional mechanical harvesting methods prove ineffective. By integrating the specific characteristics of mugwort cultivation, the harvester is designed as an efficient and scalable solution for large-scale mechanized harvesting. By integrating the unique characteristics of mugwort cultivation, this study focuses on the design and development of key components, including the crawler-driven chassis, tine drum mechanism, and hydraulic system. The main contributions of this study are as follows:

1. Based on the cultivation patterns and inherent physical properties of mugwort, a tine drum structure was designed, and a force analysis was conducted on the tine structure to determine the optimal design and tine arrangement. The kinematics of the tines were also studied. Using RecurDyn 2023 software, the motion trajectory of the tines was simulated, and post-processing was performed with the Post module to determine the optimal speed range for efficient operation, thus improving work efficiency.
2. A hydraulic system was designed, with detailed calculations and component selection for the hydraulic cylinders, motors, pumps, and other hydraulic components, ensuring the system met the performance requirements and provided robust power support for the harvester.
3. A mathematical model was established between experimental factors and performance indicators through an orthogonal rotational center combination experiment. Based on Design-Expert 13 software analysis, the optimal parameter combination was determined.

These efforts are intended to support the modernization of the mugwort industry while advancing sustainable agricultural practices.

2. Machine Structure and Working Principle

2.1. Agronomic Requirements and Plant Characteristics

Mugwort is an herbaceous plant that is highly sensitive to waterlogging. It grows best on sloping terrains and ridges, which allow good drainage and help prevent root rot.

The mugwort samples in this study were mature plants harvested from Qichun County, Hubei Province. These plants were grown with a planting spacing of 39–61 mm and a ridge width of 1600 mm, as shown in Table 1. The recommended harvesting method involves collecting fresh mugwort leaves while leaving a small amount of withered yellow leaves on the plants, as shown in Figure 1.

Table 1. Main physical parameters of mugwort plants.

Item	Numerical Value	Mean Value
Plant spacing (mm)	39–61	50
Mugwort plant height (mm)	630–1570	1030
Stem diameter (mm)	3–8.7	5.93
Mugwort diameter (mm)	40–220	130
Height of withered leaves (mm)	39–61	50

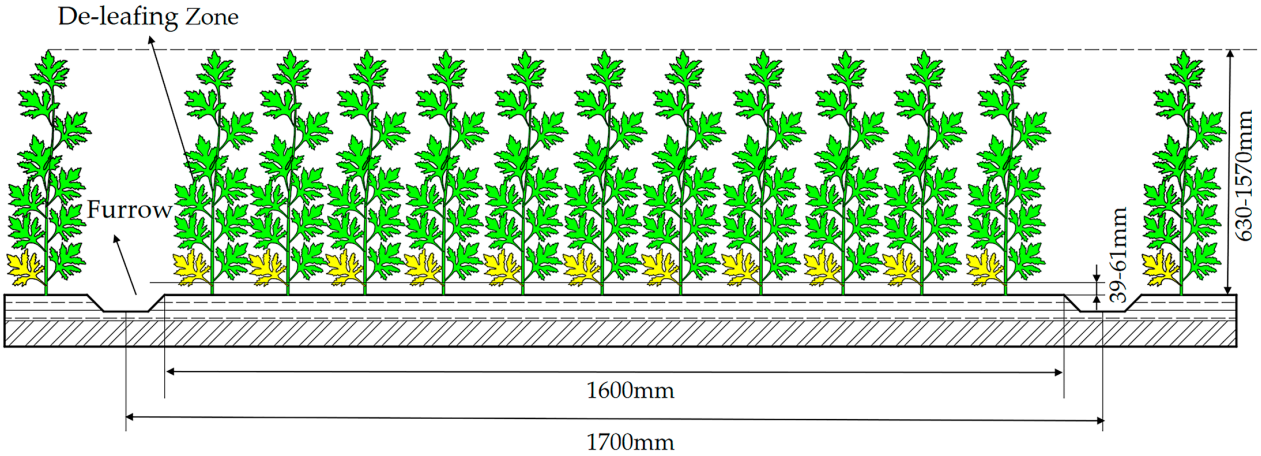

Figure 1. Harvest status of mugwort.

2.2. Design of the Harvester

As shown in Figure 2, the three-dimensional schematic structure of the mugwort harvester mainly consists of the harvesting platform, the tracked chassis, and the internal components of the vehicle body. The harvesting platform, located at the front, comprises the tine drum, the transverse conveyor belt, the lifting conveyor belt, the pressure sheaves, and the support wheels, enabling efficient harvesting and transportation of mugwort leaves. The tracked chassis includes a diesel engine, plunger variable pump, and crawler traveling mechanism, providing power to the operational devices and traveling system.

Instead of a traditional driving position and control console, the harvester is equipped with a remote-control system to operate all functions. This design minimizes the machine's size, reduces its weight, enhances operational flexibility, and significantly alleviates the operator's workload. The remote-control system consists of a transmitter, signal receiver, signal processor, and drive circuit. It uses the F24-60 dual-joystick remote from the Lee Telecrane series, operating at 310.3–331.165 MHz with a control range of up to 200 m. The controller is built around an STM32G030C8T6 microcontroller, integrating a power conversion module, proportional amplification circuit, adjustment circuit, and communication module [12].

Auxiliary components such as the vehicle's power supply, diesel tank, hydraulic oil tank, hydraulic control valves, radiator, and the integrated control system are systematically arranged within the vehicle body. These components ensure the harvester operates efficiently and stably, while also facilitating routine maintenance and repairs.

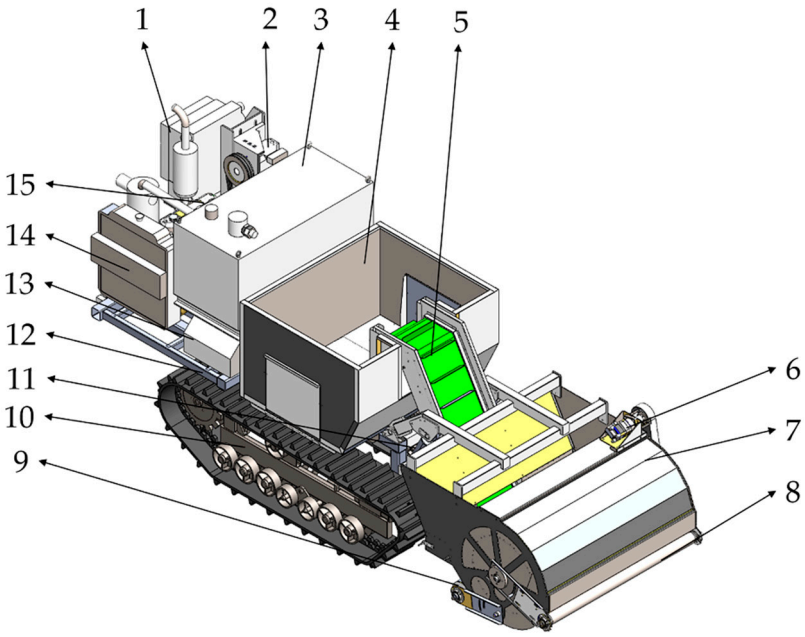

Figure 2. Structure of the whole machine of the mugwort harvester. 1. Radiator. 2. Hydraulic pump. 3. Hydraulic oil tank. 4. Material bin. 5. Lifting conveyor belt. 6. Roller hydraulic motor. 7. Tine drum cover. 8. Pressure sheave. 9. Support wheel. 10. Crawler traveling mechanism. 11. Hydraulic cylinder. 12. Frame. 13. Diesel tank. 14. Engine radiator. 15. Diesel engine.

2.3. Mechanism of Harvesting

The mugwort harvester adopts a fully hydraulic drive design. As shown in Figure 3, its working principle is as follows: the harvesting platform moves forward along the furrows with the crawler chassis, where the pressure wheels tilt the mugwort, and the fast-rotating tine drum brushes the leaves. Under the action of centrifugal force, the leaves are thrown tangentially onto the transverse conveyor belt and subsequently transported to the material bin by the lifting device, completing the harvesting process. During this process, the stubble is preserved to allow regeneration of branches and leaves, enabling multiple harvests over a three-year period.

Figure 3. Harvesting schematic diagram of the mugwort.

It should be noted that key component parameters, such as the height of the harvesting platform and the rotational speed of the tine drum, are adjustable. This adaptability ensures the harvester meets the requirements of different planting agronomies, growth stages, and mugwort varieties. Table 2 lists the main technical parameters of the fully hydraulic, crawler-type, remote-controlled mugwort harvester designed for hilly and mountainous regions.

Table 2. Main technical parameters of the mugwort harvester.

Item	Design Parameters
Overall dimensions (L × W × H) (m × m × m)	4.37 × 1.80 × 1.85
Total mass of the machine (kg)	3000
Travel mode	Remote-controlled
Working width (mm)	1700
Working rows	1
Driving speed (m/s)	0–1.5
Driving and operation speed adjustment method	Hydraulic continuously variable transmission
Engine displacement (L)	3.261
Engine Power (kW)	74.5

3. Key Mechanical Structure Design and Parameterization

3.1. Crawler Traveling Mechanism

As shown in Figure 4, the working principle of the tracked chassis involves looping continuous rubber tracks around the driving wheels and a series of rollers. The driving wheels propel the tracks, generating a rolling motion that drives the chassis forward while minimizing slippage [13,14]. Key structural parameters of the tracks, including pitch, width, grounding length, and the pitch circle diameters of the driving and supporting wheels, were meticulously calculated to optimize traction and stability.

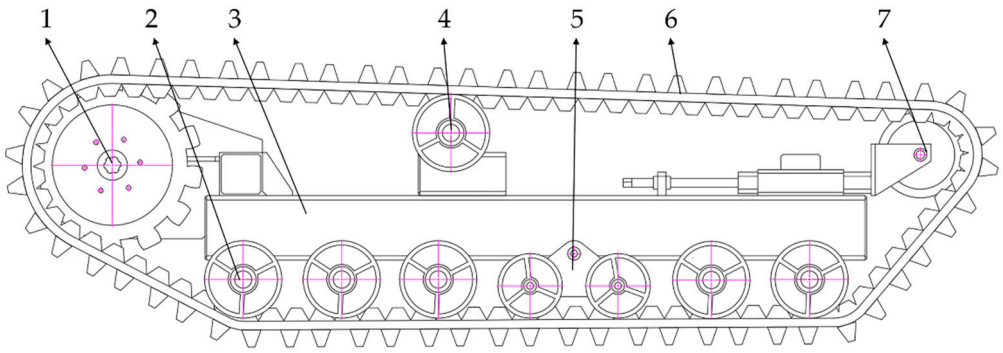

Figure 4. Schematic diagram of the crawler traveling mechanism. 1. Driving wheel 2. Supporting wheel 3. Bottom beam 4. Carrier wheel 5. Floating wheel 6. Track 7. Guide wheel.

The field traversal performance of the harvester was evaluated based on the predominant soil type in Qichun County, Hubei Province, where mugwort is widely cultivated. The soil in this region is primarily composed of red loam, which is a well-drained, stable, and firm soil type. Given these characteristics, as well as the absence of waterlogging or muddy conditions during operation, the tracked design does not require adjustments for muddy field conditions. Instead, the design focused on ensuring stability and traction on sloped terrains, which are typical of mugwort cultivation areas [15].

The use of rubber tracks enhances ground contact and reduces soil compaction, making it highly suitable for such terrains. This soil-specific adaptation aligns with the operational requirements of hillside environments, where the flexibility and stability provided by rubber tracks are critical for efficient and reliable performance.

The track pitch varies with the total mass of the machine [16–18] and is calculated using the following formula:

$$t_0 = (12 \sim 14.5)\sqrt[4]{m} \quad (1)$$

where t_0 is the track pitch, mm; m is the total mass of the machine, kg.

The track plate width b is calculated as:

$$b = (0.9 \sim 1.3) \times 209\sqrt[3]{m \cdot 10^{-3}} \quad (2)$$

The track grounding length L_1 must correspond to the track plate width b, and is calculated by:

$$L_1 = \frac{b}{\lambda'} \tag{3}$$

where λ' is a scaling coefficient, taken as 0.185.

The track gauge B is calculated as:

$$B = (3.5 \sim 4.5)b \tag{4}$$

The number of teeth on the drive wheel is 13, and the pitch circle diameter D_k of the drive wheel is calculated as:

$$D_k = \frac{t_0}{\sin\frac{180^\circ}{Z}} \tag{5}$$

where Z is the number of teeth on the drive wheel.

The guide wheel is installed at the front end of the track unit to prevent the track from misaligning and falling off. The guide wheel diameter D_t is calculated as:

$$D_t \approx (0.8 \sim 0.9)D_k \tag{6}$$

There are five supporting wheels, supported by multiple pivots and evenly distributed along the bottom of the track. The pitch circle diameter (d_z) of the supporting wheels is calculated using the following formula:

$$d_z \approx (0.5 \sim 1)D_t \tag{7}$$

The main parameters of the crawler traveling mechanism, as calculated from Equations (1)–(7), are listed in Table 3.

Table 3. Crawler structural parameters.

Item	Design Parameters
Track grounding length L_1 (mm)	1470
Track plate width b (mm)	270
Crawler gauge B (mm)	1080
Crawler pitch t_0 (mm)	90
Drive wheel pitch diameter D_k (mm)	376
Diameter of guide wheel D_t (mm)	300
Pitch diameter of supporting wheel d_z (mm)	150
Single-side track size (L × W × H) (mm × mm × mm)	2225 × 270 × 450

3.2. Harvesting Table Structure Design and Analysis

3.2.1. Limited Grafting Rate

The core structure of the mugwort harvester, shown in Figure 5, consists of key components including the pressure sheaves, support wheels, tine drum, hydraulic motor, transverse conveyor belt, and lifting conveyor belt. In harvesting applications, comb-type tines with similar functions can be classified into several types based on structural differences, such as tine drums, comb-tine drums, and spike-tine drums.

In terms of harvesting performance, the comb-tine type is prone to clogging due to plant material blocking the gaps between the tines, while the spike-tine type is more likely to cause crop damage. Therefore, for the harvesting of fresh mugwort leaves, a tine drum (Figure 5), driven by a hydraulic motor, is used for rotary leaf detachment. Unlike wheat or rice, the surface tissues of leafy plants are highly susceptible to damage [19]. The tine drum structure not only achieves efficient defoliation but also minimizes clogging and leaf damage [20–22].

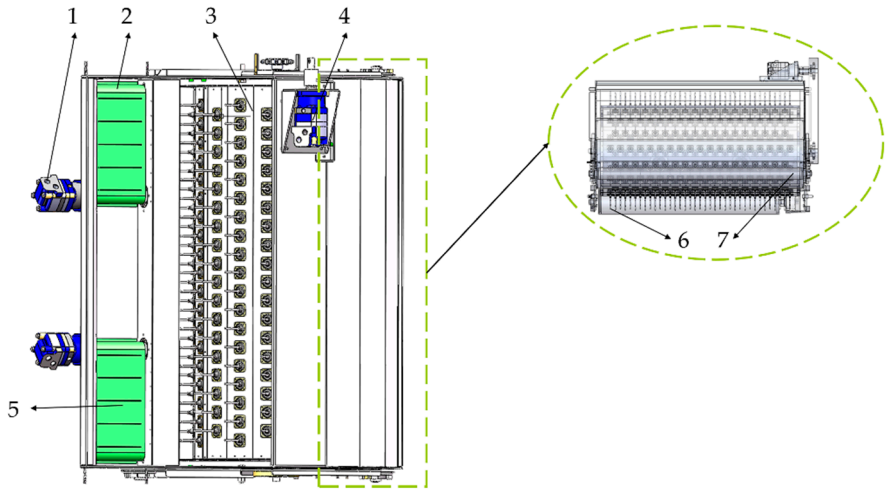

Figure 5. Sketch of the structure of the tine drum defoliation unit. 1. Hydraulic motor for transverse conveyor belt. 2. Transverse conveyor belt (left). 3. Tine drum. 4. Hydraulic motor for tine drum. 5. Transverse conveyor belt (right). 6. Support wheel. 7. Pressure sheave.

3.2.2. Determination of the Tine Drum Size

Mugwort leaves are uniformly distributed along the stem. To ensure that the harvesting area covers all regions where the mugwort leaves are present, the radius from the tip of the tines on the drum to the shaft center (referred to as the tine drum radius R) must be adapted to the physical characteristics of the plant [22,23]. The radius is determined by factors such as the height of the pressure sheave relative to the mugwort plant, the height of the withered leaves, and the contact position between the tines and the bottom leaves. To ensure that defoliated mugwort leaves remain on the drum and are transported to the upper carrying conveyor area through inertia, the contact point between the tines and the bottom leaves should form an angle β with the lowest point of the tines. Additionally, the lowest end of the tines must be positioned higher than the height of the withered leaves. To avoid soil scraping, a clearance must be maintained between the lowest point of the tines and the ground, satisfying the following formula:

$$\cos\beta \geq \frac{R - H_1}{R} \tag{8}$$

where H_1 is the height of the withered leaves of mugwort, mm.

To ensure that the radius of the tine drum covers the entire area of fresh leaves on the mugwort plant, the following equation must be satisfied:

$$R\cos\beta \geq H_4 \tag{9}$$

where H_4 is the height of the center of the flattened mugwort, mm.

The range of values for the radius R of the tine drum is determined as follows [24]:

$$\frac{H_4}{\cos\beta} \leq R \leq \frac{H_1}{1 - \cos\beta} \tag{10}$$

At this time, the height of the lowest point of the tine drum teeth from the ground is:

$$H_3 = H_1 - (R - R\cos\beta) \tag{11}$$

where H_3 is the height of the lowest point of the tine drum teeth from the ground, mm.

According to the physical parameters measured and recorded in Table 1, the harvestable range length H_4 of fresh mugwort leaves flattened by the pressure sheave wheel

is 300 mm, while the height H_1 of the withered leaves is taken as the maximum value of 61 mm. The angle β can be calculated using Equation (10), and it must be less than 33°. According to Equation (11), when the radius R of the tine drum is fixed, a larger β results in a smaller height from the ground. Therefore, β should not be too large, and it is set to 20° in this design.

The range of the tine drum radius R is 319.3–1011.5 mm. When β = 20° and the height from the ground is 40 mm, considering the overall structural dimensions, the tine drum radius is selected as 400 mm. The row width of mugwort planting is 1600 mm, as shown in Figure 6. To ensure the harvesting of a single row in one pass, the axial length of the defoliation drum is designed to be 1700 mm.

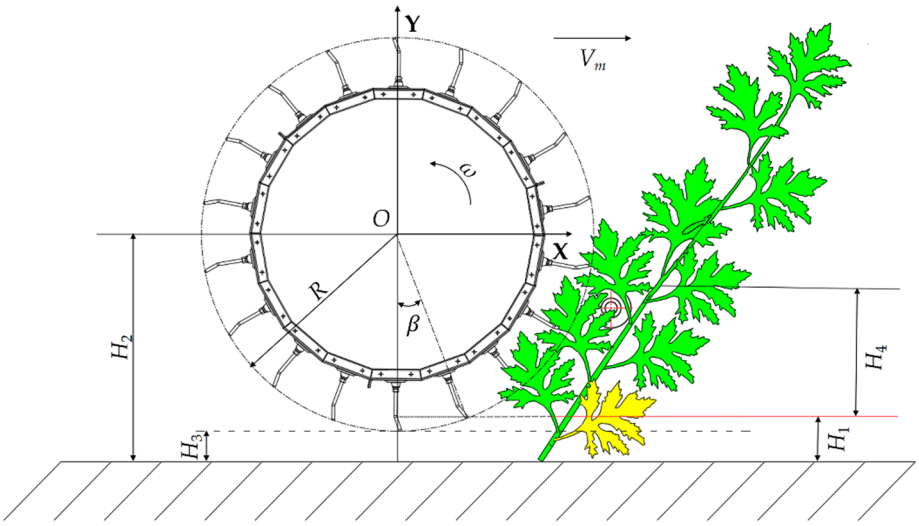

Figure 6. Schematic diagram of tine drum harvesting.

3.3. Design of Defoliation Teeth

3.3.1. Distribution of Teeth

As shown in Figure 6, mugwort leaves primarily grow around the main stem. To ensure that each plant is combed cleanly during operation, it is necessary to strike the growth area of the leaves multiple times [25,26]. The time (t') for the drum to pass through the mugwort leaf growth area can be expressed as:

$$t' = \frac{W_l}{V_m} \tag{12}$$

where W_l is the width of the mugwort leaf growth area, cm.

During this time, the drum rotates through an angle (α) given by:

$$\alpha = \frac{2\pi\omega' t'}{60} \tag{13}$$

where ω' is the angular speed of the drum, rad/s.

If each mugwort plant can be cleaned after k strikes of the tine drum teeth, the relationship between the total number of rows of teeth (H) and k can be expressed as:

$$H = \frac{2\pi k}{\alpha} = \frac{60kv}{W\omega'} \tag{14}$$

Referring to Table 1, the width of mugwort is set to 13 cm, and the forward speed of the machine is 0.8 m/s. The total number of rows of teeth is directly proportional to the number of strikes and inversely proportional to the drum speed. Preliminary tests

showed that when the linear speed of the drum teeth exceeds 13 m/s, the breakage rate of mugwort leaves significantly increases. Therefore, the drum speed is set to a lower value of 200 r/min, at which point H can be expressed as:

$$H = 3k \tag{15}$$

Given the dense distribution of mugwort planting, k is set to a higher value of 6, resulting in a total of 18 rows of teeth on the drum.

To achieve the simultaneous harvesting of a ridge, the initial distance (d) between two adjacent teeth is set to 65 mm, arranged in a straight line. As shown in Figure 7, the drum surface is evenly distributed with 18 rows of teeth along its circumference, with adjacent rows staggered. The elastic teeth are fixed to the drum's outer wall using rivets, and their bases are wrapped with rubber sleeves to ensure durability and structural integrity [27].

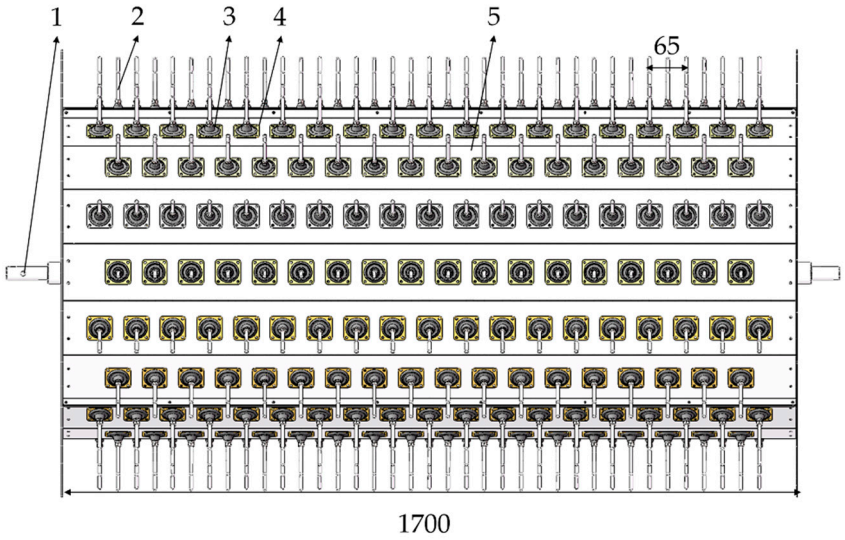

Figure 7. Schematic diagram of the tine drum structure. 1. Drum shaft. 2. Elastic teeth. 3 Vulcanized rubber. 4. Elastic teeth fixed base. 5. Drum.

3.3.2. Defoliation Range and Inclination Angle of Elastic Teeth

As shown in Figure 8, the defoliation range (L) is defined as the distance from the circular tip of the elastic teeth to the vulcanized rubber at the tooth root. If the defoliation interval is too small, mugwort plants may be overly compressed, increasing the breakage rate and reducing the net rate of mugwort leaf harvesting. If the interval is too large, the contact frequency between the leaves and the elastic teeth decreases, which also lowers the net leaf harvesting rate.

Thus, the defoliation interval must match the height of the mugwort plant stem that is tilted and pressed near its root by the pressure sheave. Field measurements indicate that this height typically ranges between 90 mm and 130 mm. Based on these measurements, the defoliation range is set at L = 110 mm in this design.

As shown in Figure 8, the angle θ formed between the axis of the spring wire at the end of the defoliation elastic tooth and the line connecting the center of the elastic tooth drum is the inclination angle of the elastic tooth [28] (positive for forward inclination, negative for backward inclination). This angle directly impacts the defoliation effectiveness. When the position angle γ is between 0° and 90°, the mugwort plant is in the defoliation stage. At this time, the force on the mugwort leaf in the x-axis direction is given by:

$$\sum F_x = F_c \cos\theta - f \sin\theta - G \sin\gamma \tag{16}$$

where

$$f = \mu F_c \tag{17}$$

where F_c is the support force of the elastic tooth on the ai leaf, N; f is the friction force between the elastic teeth and the mugwort leaf, N; G is the gravitational force of the mugwort blade, N; μ is the static friction coefficient of the elastic tooth, N.

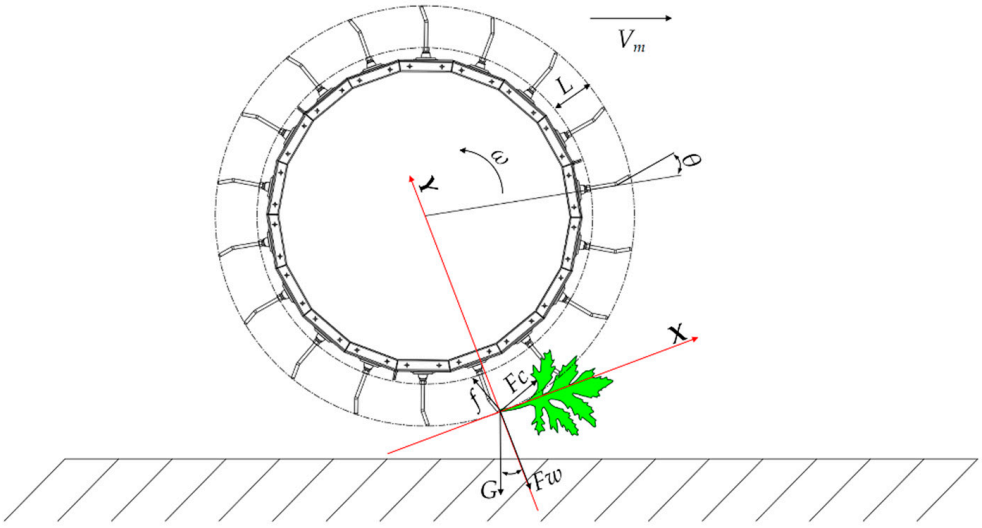

Figure 8. Structure and force analysis of defoliation elastic teeth.

According to Equation (16), as the inclination angle θ of the defoliation elastic teeth increases, the net force ($\sum F_x$) on the mugwort leaf along the x-axis decreases. This results in a reduction in the carrying energy exerted by the elastic teeth on the mugwort leaves, making it less favorable for effective defoliation of the mugwort plant.

When the position angle γ is located between $-90°$ and $0°$, the mugwort leaf enters the detachment stage. At this case, the force on the leaf along the y-axis is given by:

$$\sum F_y = F_c \sin\theta + f\cos\theta - G\cos\gamma - F_w \tag{18}$$

According to Equation (18), as the inclination angle (θ) increases, the net force ($\sum F_y$) on the mugwort leaf along the y-axis decreases. which enhances the carrying energy, making it more favorable for leaf detachment.

From the above analysis, it can be observed that there is a trade-off between the defoliation ability and the detachment ability of the defoliation elastic teeth. Based on the design experience from reference [29], the inclination angle of the defoliation elastic teeth is typically selected within the range of $0°$ to $30°$. Combining the results from multiple experiments, the inclination angle (θ) is set to $20°$ in this design.

3.4. Motion Analysis of Elastic Teeth

During the forward movement of the harvester, the tine drum undergoes a composite motion consisting of both linear and rotational movements. The motion of the tine drum is shown in Figure 6. Assume the center of the drum is the origin O, the forward direction of the harvester is along the positive x-axis, and the vertically upward direction is along the positive y-axis. A rectangular coordinate system is established accordingly. The displacement trajectory equation of an arbitrary elastic tooth endpoint (M_0) at time (t) is expressed as follows [30]:

$$\begin{cases} x = V_m t + R\cos(\omega t) \\ y = H_2 + R\sin(\omega t) \end{cases} \tag{19}$$

where v_x is the horizontal partial velocity of an end point of the elastic tooth, m/s; v_y is the vertical velocity of an endpoint of the elastic tooth, m/s.

Taking the first-order derivative of the displacement equation, the partial velocities in the x- and y-directions at the endpoint (M_0) of any elastic tooth can be expressed as:

$$\begin{cases} v_x = V_m - R\omega \sin(\omega t) \\ v_y = R\omega \cos(\omega t) \end{cases} \tag{20}$$

where v_x is the horizontal partial velocity of an end point of the elastic tooth, m/s; v_y is the vertical velocity of an endpoint of the elastic tooth, m/s.

The combined velocity (v) at the endpoint (M_0) of any elastic tooth is calculated by substituting into the combined velocity equation as:

$$v = \sqrt{v_x^2 + v_y^2} = \sqrt{V_m^2 + (R\omega)^2 - 2R\omega V_m \sin(\omega t)} \tag{21}$$

The trajectory of an endpoint of the elastic tooth relative to the ground depends on the ratio (λ) between the linear velocity of an endpoint on the elastic tooth and the forward speed of the harvester. The trajectories of the drum corresponding to different values of λ are shown in Figure 9.

$$\lambda = \frac{V_S}{V_m} = \frac{\omega R}{V_m} \tag{22}$$

where V_s is the linear velocity of an endpoint of the elastic tooth, m/s.

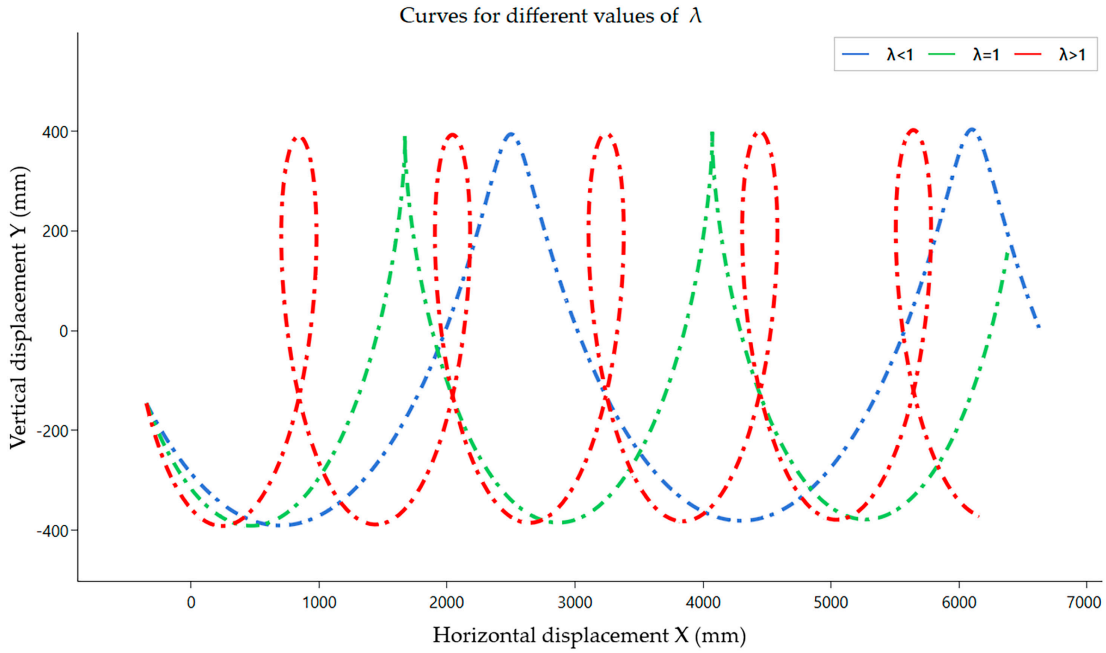

Figure 9. Different trajectories of the elastic tooth drums.

The parameter λ significantly affects the trajectory of the elastic tooth. As shown in Figure 9, the motion trajectory of the endpoint of the elastic tooth is simulated using RecurDyn 2023 software. The trajectory changes with variations in λ, resulting in three distinct motion trajectories for the cases $\lambda > 1$, $\lambda = 1$, and $\lambda < 1$.

To ensure the roller combs the mugwort leaves and throws the leaves onto the conveyor belt, the elastic tooth drum must possess a horizontal partial velocity. When $\lambda > 1$, the condition $v_x < 0$ occurs [31], allowing the mugwort leaves to be effectively thrown.

3.5. Force Analysis of Elastic Teeth

The bending moment (M) acting on the elastic tooth can be expressed as [29]:

$$M = LF \tag{23}$$

where F is the combined force on the elastic tooth, N.

The deflection y at the endpoint of the elastic tooth is given by:

$$y = \frac{L^3 F}{3EI} \tag{24}$$

where

$$I = \frac{\pi d_t^4}{64} \tag{25}$$

where E is the modulus of elasticity of the elastic tooth material, Mpa; I is the moment of inertia of the elastic tooth cross-section, mm^4; d_t is the diameter of elastic tooth, mm.

The maximum static stress σ is:

$$\sigma = \frac{M}{W} = \frac{LF}{W} \tag{26}$$

where

$$W = \frac{\pi d_t^3}{32} \tag{27}$$

where W is the bending section coefficient, mm^3.

The material of the elastic tooth is 65Mn spring steel, with a Young's modulus of 210 GPa, a force arm L of 110 mm, and diameter d_t of 5 mm. The combined force acting on the elastic tooth mainly originates from overcoming the connecting force between the mugwort leaves and stems. According to the literature [11,32], the maximum harvesting force varies with the stretching angle (0°, 30°, 45°, 60°, and 90°) as follows: 8.77–11.75 N, 7.81–15.69 N, 8.4–20.89 N, 8.99–17.99 N, and 6.39–11.08 N, respectively. Since this study employs a bottom-to-top defoliation method, consistent with the growth pattern of mugwort plants, the maximum stem–leaf harvesting force of 20.89 N at 45° was selected.

Based on the force analysis, the simplified model of the elastic tooth was imported into ANSYS 2022 finite element analysis software. The material used was 65Mn, and its properties were assigned. The surface of the elastic tooth was meshed, and boundary conditions such as loads were applied. The simulation results are as follows:

Figure 10a shows the total deformation analysis. The maximum deformation occurs at the endpoint of the elastic tooth, with a maximum deformation value of 0.2651 mm.

Figure 10b shows the strain analysis. The maximum equivalent strain occurs at the connection between the elastic tooth and the nut, with a maximum strain value of 1.3566×10^{-3}.

Figure 10c shows the equivalent stress analysis. The maximum equivalent stress occurs at the connection between the elastic tooth and the nut, with a maximum stress value of 284.08 MPa, which is below the permissible stress of 65Mn material (σ_b = 780–980 MPa).

According to the simulation results, the design meets the working requirements of the elastic tooth.

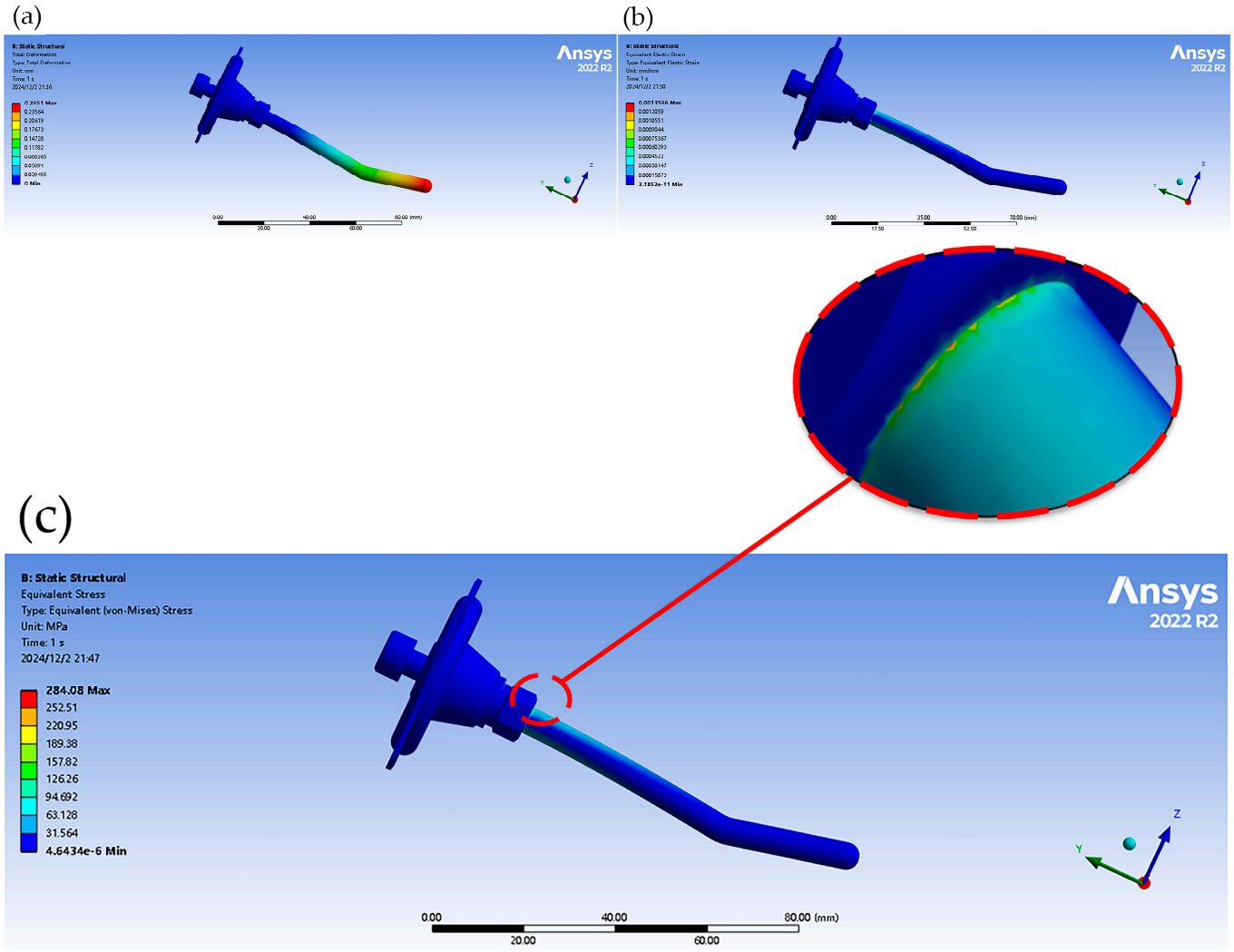

Figure 10. (**a**) Total deformation cloud diagram of the elastic tooth model; (**b**) equivalent strain cloud diagram of the elastic tooth model; (**c**) equivalent stress cloud diagram of the elastic tooth model.

4. Hydraulic Transmission and Track Drive Unit Design

4.1. Hydraulic System Principle Design

Compared to a traditional mechanical transmission, a hydraulic transmission allows for stepless speed regulation. Under the same power conditions, hydraulic systems are smaller and more compact, leading to a more efficient overall mechanical structure. The hydraulic oil supply system of the harvesting table adopts an open-loop hydraulic circuit, with actuators, including a rotary hydraulic motor and hydraulic cylinders, performing the desired functions. The detailed schematic of the hydraulic system is shown in Figure 11.

The mugwort fresh leaf harvester is a typical agricultural walking machine. Based on the working pressure range of different equipment [31], the system design pressure for agricultural machinery ranges from 7 MPa to 21 MPa. For this study, the hydraulic system pressure is selected to be 16 MPa.

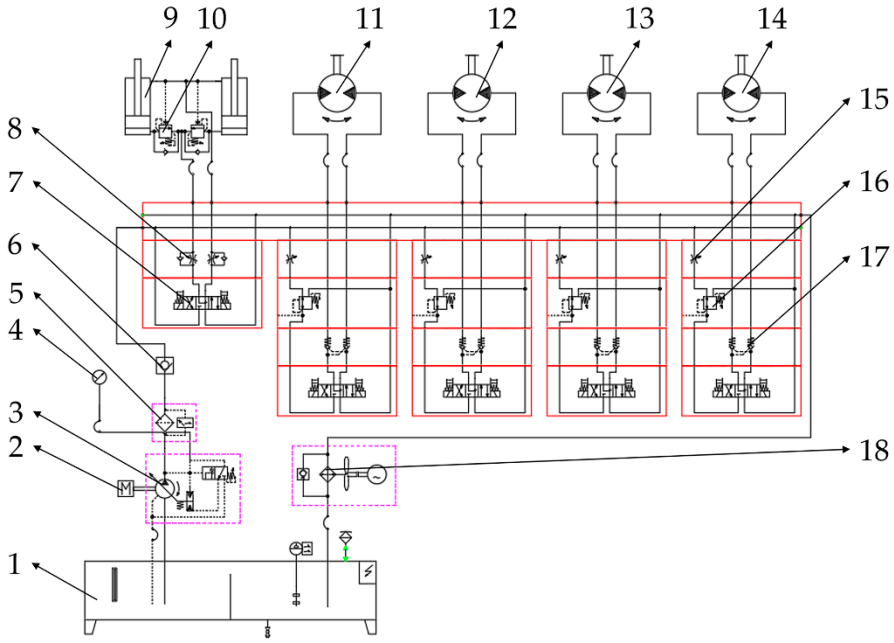

Figure 11. Hydraulic drive schematic diagram of the mugwort harvester. 1. Hydraulic oil tank. 2. Engine. 3. Constant pressure variable pump. 4. Vibration-resistant pressure gauge. 5. Filter. 6. Check valve. 7. Three-position four-way electromagnetic directional valve. 8. One-way throttle valve. 9. Cutter implement lifting cylinders. 10. Balancing valve. 11. Roller hydraulic motor. 12. Transverse conveyor hydraulic motors (left). 13. Transverse conveyor hydraulic motors (right). 14. Lifting and conveying hydraulic motor. 15. Speed regulating valve. 16. Pressure-reducing valve. 17. Two-way hydraulic lock. 18. Air cooler.

4.2. Determination of Major Actuator Parameters

4.2.1. Determination of Hydraulic Drive Parameters for the Elastic Tooth Drum

The elastic tooth drum is driven by a hydraulic motor through chain transmission. The drum has a diameter of 800 mm and an axial length of 1700 mm. The analysis is based on the harvesting capacity of the drum and the material conveying capacity of the conveyor belt for whole ridge harvesting.

From the analysis of Figure 12 above, the torque equation of the drum is given by [33]:

$$T = \int_0^{\frac{l}{d_t}} M_f + (F_a R_a + T_a) + (F_b R_b + T_b) + (F R_c + T_c) dx \tag{28}$$

where M_f is the torque exerted by the elastic tooth fixation seat on the drum axis, N·m; F_a is the gravitational force of the mugwort leaves, N; F_b is the support force of the plant on the drum, N; l is the operating width of the drum, mm; R_n is the radius of the roller, mm; R_a, R_b, R_c are the force arms of each force on the center of the drum axis, mm; T_a, T_b, T_c are the moments of inertia of each force on the center of the drum axis, N·m.

The mugwort leaves, after being picked by the elastic teeth, are subjected to the rotational inertia force of the drum and gravity, which throws the leaves onto the conveyor belt behind. Assuming that each mugwort leaf unit is a rigid body, the mass inertia force on the drum can be decomposed into the normal inertia force (F^n) and the tangential inertia force (F^t). Since the harvesting drum moves uniformly in operation [30], its angular acceleration is zero, meaning the tangential inertia force due to the gravity of the leaves is also zero. The above analysis leads to the following equation:

$$\begin{cases} T_a = F^n \cdot R_1 = m_a R_1^2 \omega^2 \\ T_b = T_c = 0 \end{cases} \tag{29}$$

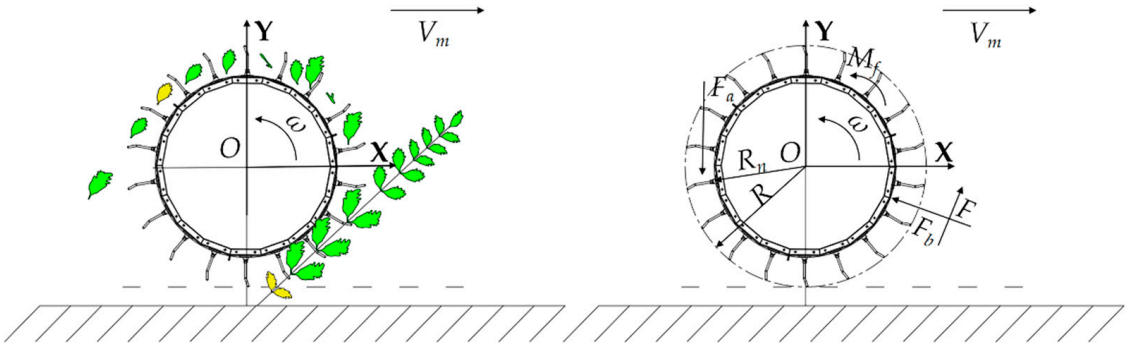

Figure 12. Sketch of the force on the elastic tooth roller.

Assuming that the force on the elastic tooth is uniformly distributed, the center of the tooth is selected as the force application point, Therefore, $R_1 = R_n + (R - R_n)/2$, which can be brought into Equation (29).

$$\begin{cases} T_a = \frac{m_a}{4}\omega^2(R_n + R)2 \\ T_b = T_c = 0 \end{cases} \tag{30}$$

By substituting Equation (30) into Equation (29), the drum torque can be expressed as:

$$T = \int_0^{\frac{l}{d_t}} M_f + \frac{m_a}{4}\omega^2(R + R_n)^2 + (F_a + F) + (R_n + \frac{R - R_n}{2})dx \tag{31}$$

The torque (M_f) exerted by the fixed base of the unit elastic tooth on the axis is 2.2972 N·m. The force (F) required to overcome the leaf–stem fracture connection is 20.89 N. The average weight of a mugwort leaf is 0.5 g. According to the literature [34], the drum speed ranges from 160 to 240 r/min, with the best defoliation effect verified at 200 r/min. Substituting the parameters into Equation (31), the load torque of the drum motor is 338 N·m.

The hydraulic motor transmits driving force to the tine drum through a chain transmission, as illustrated in Figure 13. The displacement (V_a) of the hydraulic motor for the tine drum is calculated using the following formula:

$$V_a = \frac{2\pi T}{p\eta_m} \tag{32}$$

where T is the load torque of the hydraulic motor, N·m; p is the working pressure of the hydraulic motor, Mpa; η_m is the hydraulic motor mechanical efficiency, η_m = 0.95.

By substituting the relevant data into Equation (32), the drum hydraulic motor displacement is calculated as 139.7 mL/r. The selected motor model is a BM5-160, with a maximum continuous speed of 430 r/min, a displacement of 160 mL/r, and a maximum continuous working pressure of 17.5 MPa.

During the mugwort leaf harvesting process, the roller moves at a constant speed, so the working flow rate of the hydraulic motor is determined by the following equation:

$$q_M = n_t \cdot V_a \tag{33}$$

where q_M is the motor working flow, L/min; n_t is the motor speed, r/min.

From this, the operating flow rate of the roller hydraulic motor is calculated to be 33.6 L/min.

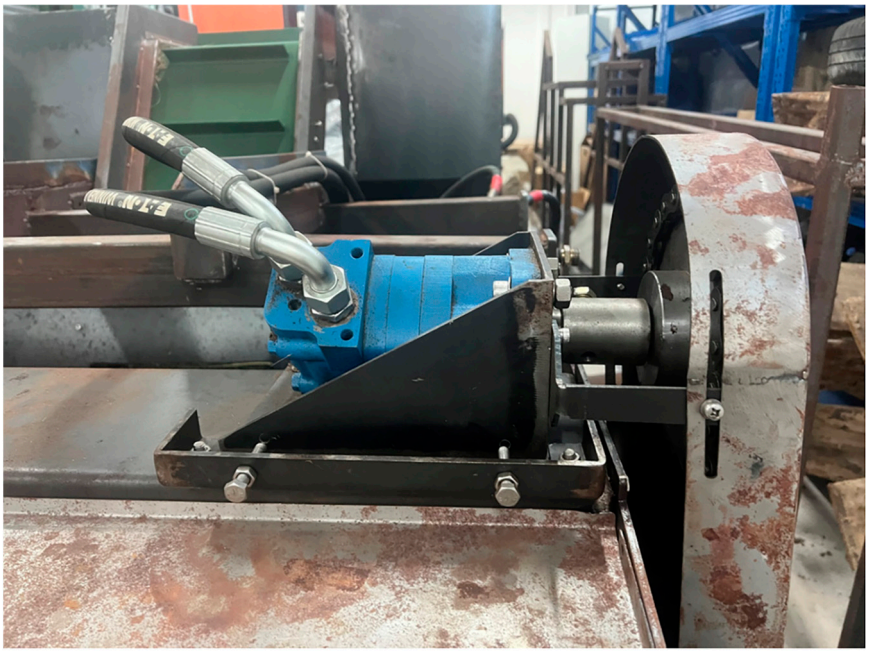

Figure 13. Installation diagram of the tine drum hydraulic motor.

4.2.2. Hydraulic Motor for Transverse Conveyor

To ensure that the large volume of fed mugwort leaves is transported to the silo in a timely manner without clogging on the conveyor belt, and to prevent the lifting conveyor belt from being excessively wide and impacting the structure of the cutting table, the machine is equipped with left and right transverse conveyor belts, as shown in Figure 14.

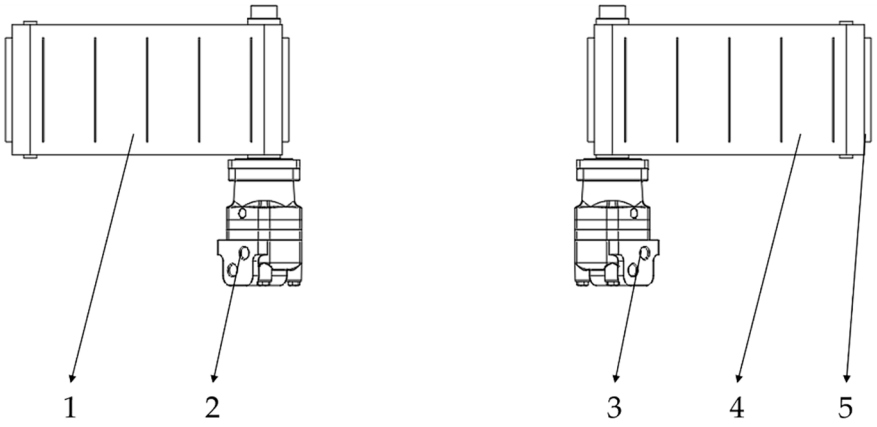

Figure 14. Hydraulic motor for transverse conveyor belt. 1. Transverse conveyor belt (left). 2. Hydraulic motor for transverse conveyor (left). 3. Transverse conveyor belt (right). 4. Hydraulic motor for transverse conveyor (right). 5. Flap-type conveyor belt.

In the design and installation, the hydraulic motor is directly connected to the conveyor belt roller via a coupling. As a result, the conveyor belt roller speed is equal to the motor output speed. According to the harvesting efficiency requirements, a conveyor belt speed of 0.5 m/s is considered appropriate. The diameter of the conveyor belt roller is 50 mm. The transverse conveyor belt roller speed n_{s1} is given by the following formula:

$$n_{s1} = \frac{v_{s1}}{\pi d_{s1}} \tag{34}$$

where v_{s1} is the transverse conveyor belt linear speed, m/s; d_{s1} is the diameter of the transverse conveyor belt roller, mm.

From Formula (34), the conveyor drum speed is calculated to be 191 r/min, which means the conveyor belt hydraulic motor speed is also 191 r/min. According to the BM5 series hydraulic motor parameter table, the motor torque is 160 N·m [31]. Substituting this into Formula (32), the displacement is calculated to be 66 mL/r.

Considering the stability and smoothness requirements during operation, the selected motor model is a BM5-80, with a maximum continuous speed of 850 r/min, a displacement of 80 mL/r, and a maximum continuous working pressure of 17.5 MPa.

From Formula (33), the working flow rate of the transverse conveyor hydraulic motor is calculated to be 15.28 L/min. The same calculation method is used for the other transverse conveyor hydraulic motor, and it is not repeated in this paper.

4.2.3. Lifting and Conveying Hydraulic Motors

The lifting conveyor belt adopts a baffle-type design, as shown in Figure 15, with the conveyor belt maintaining a specific inclination angle and speed relative to the forward direction of the harvester. To ensure the smooth passage of mugwort leaves, the linear speed of the lifting conveyor belt must exceed the forward speed of the harvester [35]. The speed of the designed lifting conveyor belt meets the following conditions:

$$v_{s2} \cos \delta \geq V_m \tag{35}$$

where v_{s2} is the lifting conveyor belt line speed, m/s; δ is the angle between the conveyor and the horizontal direction, with $\delta = 35°$ taken for comprehensive consideration.

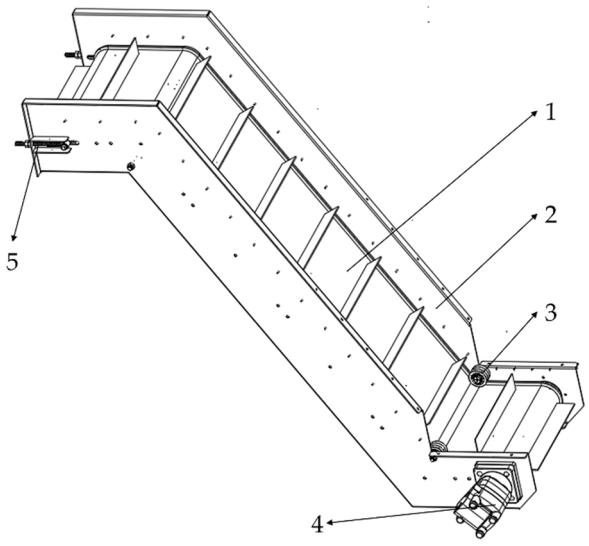

Figure 15. Schematic diagram of the lifting conveyor belt. 1. Baffle Conveyor Belt. 2. Side baffle. 3. Pressure pulley. 4. Lifting hydraulic motor. 5. Tensioning device.

Approximating the motion of the conveyor belt as circular motion yields the following equation:

$$v_{s2} = \frac{n_{s2} \pi d_{s2}}{60} \tag{36}$$

where n_{s2} is the rotation speed of the lifting conveyor belt roller, r/min; d_{s2} is the diameter of lifting conveyor belt roller, mm.

Bringing Equation (36) into Equation (35) yields:

$$n_{s2} \geq \frac{60 v_{s2}}{\pi d_{s2} \cos \delta} \tag{37}$$

Substituting the data, $n_{s2} \geq 262$ r/min. However, an excessively large d_{s2} may lead to instability in the conveyor device, potentially causing vibration. To reduce vibrations, n_{s2} is set to 262 r/min. To improve productivity, the speed of the lifting conveyor belt should not be lower than that of the transverse conveyor belt.

According to the BM5 series hydraulic motor parameter table, the motor torque is 278 N·m [31]. Substituting this value into Equation (32), the displacement is calculated as 121 mL/r. The selected motor model is a BM5-125, with a maximum continuous speed of 522 r/min, a displacement of 125 mL/r, and a maximum continuous working pressure of 17.5 MPa. From Equation (33), the working flow rate of the lifting conveyor hydraulic motor is calculated as 32.75 L/min.

4.2.4. Parameter Determination of the Lifting Hydraulic Cylinder for the Harvesting Platform

During the operation of the mugwort harvester, the piston rod of the lifting hydraulic cylinder contracts, using the front axle support shaft as a pivot point, causing the platform to slowly lower and allowing the support wheels to fit the ground for harvesting. At the same time, the height can be adjusted as needed. During non-operational times, the hydraulic cylinder raises the harvesting platform to facilitate transportation.

The basic requirements for the hydraulic cylinder include sufficient thrust and an appropriate lifting speed to move the harvesting platform up and down.

The mass of the harvesting platform is 400 kg, and the thrust F_t required for each hydraulic cylinder is calculated as follows:

$$F_t = \frac{G_c}{2\cos\theta_c} = \frac{(m_1 + m_2)g}{2\cos\theta_c} \tag{38}$$

where F_t is the hydraulic cylinder thrust, N; G_c is the weight of the harvesting table when fully loaded, N; m_1 is the mass of the cutting table implement, kg; m_2 is the mass of the mugwort leaves in the cutting table, taken as 10 kg; θ_c is the angle between the cylinder piston rod and the horizontal plane when fully extended, 76°.

The formula for calculating the inner diameter of the hydraulic cylinder is as follows:

$$D = \sqrt{\frac{4F_t}{\pi\Delta P_0\eta_0\eta_1}} \tag{39}$$

where D is the inner diameter of the hydraulic cylinder, mm; ΔP_0 is the pressure difference between the two ends of the hydraulic cylinder, MPa, with ΔP_0 = 8 Mpa [36]; η_1 is the load efficiency of the hydraulic cylinder; η_0 is the total transfer efficiency of the hydraulic cylinder.

According to the literature [37], the load efficiency of the hydraulic cylinder ranges from 0.6 to 0.75, and the total transfer efficiency ranges from 0.8 to 0.95. In this paper, the design is taken as η_1 = 0.65, η_0 = 0.85, and F_t = 8500 N. Bringing the data into Equation (39) gives the inner diameter of the hydraulic cylinder as 49.48 mm.

Hydraulic piston rod diameter calculation formula:

$$d_g = D\sqrt{\frac{\varphi_1 - 1}{\varphi_1}} \tag{40}$$

where d_g is the rod diameter of the hydraulic cylinder, mm; φ_1 is the hydraulic cylinder speed ratio.

According to the total pressure of the hydraulic system, the operating speed ratio φ_1 of the hydraulic cylinder is 1.6. Substituting into Equation (40), the hydraulic piston rod diameter is calculated to be 30.3 mm.

Based on the above theoretical calculations, the hydraulic cylinder model selected in this paper is the HSG series, and its specific performance parameters are shown in Table 4.

Table 4. Main performance parameters of cutting table lifting hydraulic cylinder.

Item	Parameter
Model number	HSGK01-63/35
Cylinder bore (mm)	63
Rod diameter (mm)	35
Stroke (mm)	200
Maximum working pressure (MPa)	21
Mounting form	Upper and lower earring connection

According to the literature [31], to reduce inertial impact, the expansion and contraction speed v_c is set at 0.12 m/s. During the lifting and lowering process of the harvesting table, the hydraulic cylinder experiences the maximum thrust when rising. Therefore, only the flow rate q_c required for the hydraulic piston rod extension needs to be considered, as follows:

$$q_c = \frac{\pi D^2 v_c}{4} \tag{41}$$

From Equation (41), the flow rate required to extend the hydraulic cylinder is calculated as 23 L/min.

4.2.5. Hydraulic Pump and Engine Selection

The power for the system actuators is supplied by a hydraulic pump [14], which is selected based on the total flow required in the hydraulic system for the actuators of the mugwort harvester. Since the track travel hydraulic system is independent, it does not need to be considered.

The working pressure of the hydraulic pump is given by:

$$P_p = P_m + \sum \Delta P \tag{42}$$

where P_p is the working pressure of the hydraulic pump, MPa; P_m is the maximum working pressure of the hydraulic system circuit; Mpa; $\sum \Delta P$ is the total hydraulic pressure loss in the system circuit from the hydraulic pump to the motor, hydraulic cylinder, and other actuating elements, MPa.

In this hydraulic system, the hydraulic pump is directly connected to the engine via the flywheel disk, ensuring its speed matches the engine speed. Considering the pressure reserve and pressure loss in the hydraulic system, the selected pressure is set at 1.25 times the working pressure, with the total pressure loss calculated as 0.25 times the maximum working pressure. The design pressure of the mugwort harvester's actuating elements is 16 MPa. According to Equation (42), the pump's working pressure is calculated as 20 MPa. Allowing for a 20% pressure reserve, the rated pressure of the hydraulic pump is selected as 24 MPa. The output flow rate of the hydraulic pump is calculated using the following formula:

$$Q_b \geq K \sum Q_{\max} \tag{43}$$

where Q_b is the flow rate of the hydraulic pump, L/min; K is the system flow leakage coefficient, taken as 1.1 in this study; $\sum Q_{max}$ is the total flow required by the hydraulic system of the actuator, L/min.

The displacement of the hydraulic pump is calculated using the formula:

$$V_b = \frac{Q_b}{n_b \eta_v} \tag{44}$$

where V_b is the hydraulic pump displacement, mL/r; n_b is the hydraulic pump rated speed, r/min; η_v is the total efficiency of the hydraulic pump, taken as 0.85 in this study.

From Equation (43), the flow rate of the hydraulic pump Q_b is calculated as 146 L/min. The Rexroth A10VSO71 piston variable pump is selected, with a rated pressure of 24 MPa, a maximum speed of 2400 r/min, and a displacement of 71 mL/r. Substituting into Equation (44), the hydraulic pump displacement is calculated as 64.8 mL/r, meeting the system's operational requirements.

The engine selection is based on the maximum output power of the entire machine during operation. The total power consumption primarily includes traveling power consumption, hydraulic system power consumption, and power consumption of other working components. Neglecting the impact of air resistance, the maximum resistance encountered by the machine while traveling under full load and uniform-speed climbing conditions is given by:

$$F_\alpha = (m + m_l)g[(f_1 + f_2)\cos\psi + \sin\psi] \tag{45}$$

where F_α is full load climbing resistance, N; m_l is the mass of mugwort leaves in the silo, kg; f_1 is the rolling resistance coefficient, taken as 0. 10; f_2 is the internal friction resistance coefficient, taken as 0.05; ψ is the maximum climbing angle, taken as 20°.

The machine was modeled using SolidWorks 2022 software, and the mass of the fully fueled machine was obtained as approximately 3230 kg using the quality assessment module. Based on preliminary experimental studies, the mass of the full silo during mugwort harvesting was about 150 kg. The climbing power can be calculated as:

$$P_\alpha = \frac{F_\alpha v_\alpha}{3600} \tag{46}$$

where P_α is the climbing power, kW; v_α is the maximum traveling speed of the whole machine at the maximum climbing degree, taken as 5 km/h.

During the working process of the harvester, the pressure and flow rate of the actuator hydraulic system change dynamically, resulting in a wide range of power variations. Therefore, the engine power is designed based on the maximum power required by the system. The total drive power required for the piston variable pump is calculated using the following formula:

$$P_g = \frac{P_p Q_{b1}}{60\eta_v} \tag{47}$$

where P_g is the driving power of the hydraulic pump, kW; Q_{b1} is the maximum flow rate of the hydraulic system, taken as 97 L/min.

The engine power rating must meet the following condition:

$$P_e \geq P_\alpha + P_g \tag{48}$$

Based on the calculation, the engine's rated power P_e must be at least 68.3 kW. Considering the need for a power reserve, the 4G33TC inline water-cooled four-stroke diesel engine produced by Changchai was selected. Its main parameters are as follows: rated power 74.5 kW, rated speed 2300–2600 r/min, total displacement 3.261 L, maximum net torque 415 N·m, and net mass of 280 kg. The schematic diagram of the track-driven chassis is shown in Figure 16.

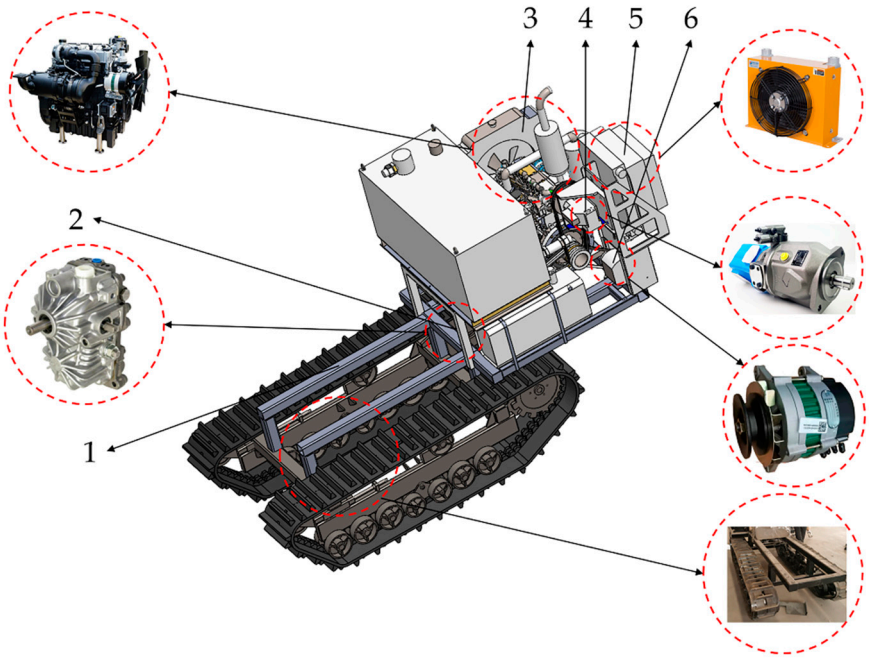

Figure 16. Schematic diagram of crawler drive chassis. 1. Chassis frame. 2. HST hydrostatic transmission. 3. Diesel engine. 4. Hydraulic pump. 5. Radiator. 6. Generator.

5. Field Experiments with Mugwort Harvester

5.1. Experimental Conditions

This experiment was conducted at a mugwort planting base located in Qichun County, Huanggang City, Hubei Province, under sunny weather conditions. The average row spacing of mugwort plants at the planting base was 50 mm, with a planting density of approximately 400 plants/m^2. The average moisture content of the mugwort leaves was 50.13%, and the plant height ranged from 650 to 1450 mm, characteristic of a typical dryland dense-planting mode for mugwort cultivation. The experimental field measured approximately 50 m in length and 35 m in width, making it suitable for mechanized harvesting operations. The experimental equipment and tools included a mugwort harvester, vernier caliper, tape measure, HT-4200 non-contact digital handheld tachometer, and a smartphone.

5.2. Experimental Factors and Indicators

Indicators affecting the performance of the mugwort harvester were selected for testing. Ideally, complete fresh leaves are required during mugwort harvesting. Therefore, this experiment selected the net rate of mugwort leaf harvesting, rate of impurity content, and rate of mugwort leaf availability as the primary indicators. These indicators were used to evaluate the working performance of the whole machine and the quality of the harvesting operation [38–40]. However, these selected indicators focus primarily on immediate harvesting performance and may not fully account for other factors that influence the overall functionality of the harvester. For example, the adaptability of the machine to different field conditions, such as variations in terrain, slopes, and crop density, was not included in this study. These aspects represent important considerations for future research to further refine the performance evaluation and expand the practical applicability of the harvester.

(1) Net Rate of Mugwort Leaf Harvesting

As shown in Figure 17, the net rate of mugwort leaf harvesting refers to the proportion of mugwort leaves detached from the stem during the harvesting process. Measurements

were taken in the designated test area, and the average value was calculated using the following formula:

$$S_j = \frac{m_y}{m_y + m_w} \times 100\% \tag{49}$$

where S_j is the net rate of mugwort leaf harvesting, %; m_y is the mass of clean mugwort leaves in the bin, g; m_w is the mass of residual mugwort leaves on the stalk, g.

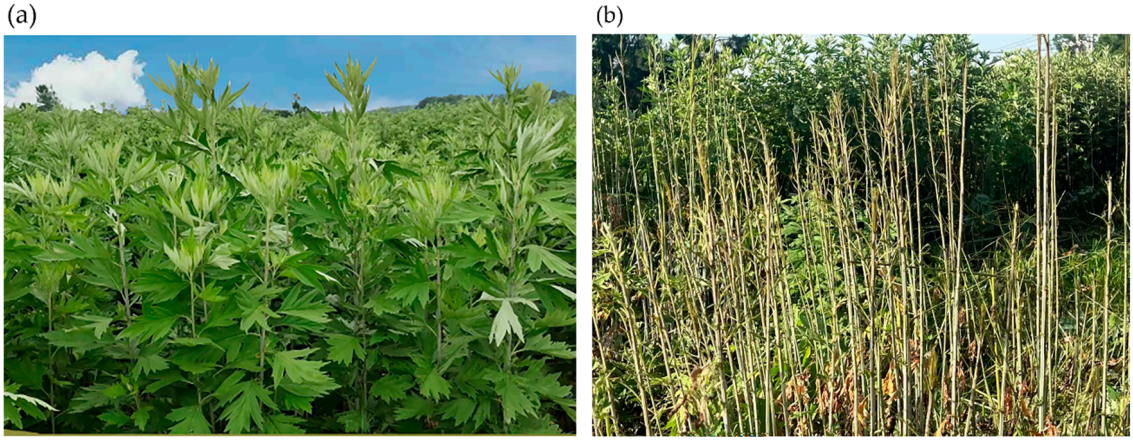

Figure 17. (**a**) Mugwort harvesting diagram of mugwort growing state; (**b**) Mugwort harvesting diagram of mugwort leaves after harvesting.

(2) Impurity Rate

The impurity rate refers to the proportion of impurities present in the leaves during the harvesting process. These impurities include weeds, stalks, branches, and other non-mugwort leaf materials, as shown in Figure 18.

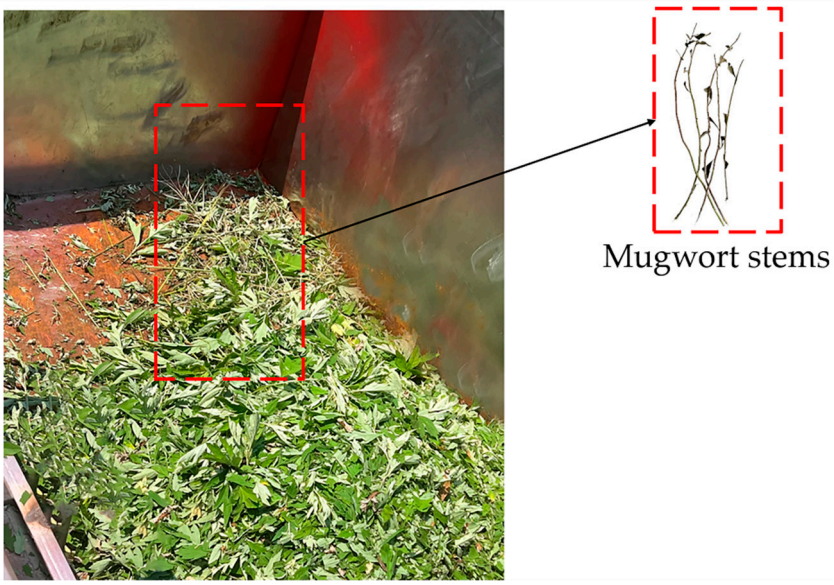

Figure 18. Impurity-containing mugwort leaves during harvesting.

The impurity rate reflects their purity and quality, serving as an important indicator for evaluating the quality of mugwort leaf products. The calculation formula is as follows:

$$Z_Z = \frac{m_z}{m_t} \times 100\% \tag{50}$$

where Z_z is the impurity content, %; m_z is the mass of impurities in the bin, g; m_t is the total mass of harvest in the bin, g.

(3) Mugwort Leaf Usability

Currently, there is no industry standard for evaluating the breakage rate of mugwort leaves. Based on the judgment criteria provided by personnel from the Qichun Mugwort Planting Company, this study categorizes harvested mugwort leaves into three grades according to leaf size and degree of breakage, as shown in Figure 19:

1. Intact mugwort leaves retain their natural, complete form without noticeable breakage or separation.
2. Partially broken leaves exhibit minor damage or splits but remain largely intact.
3. Severely broken leaves are predominantly fragmented into small pieces or powder with almost no intact parts.

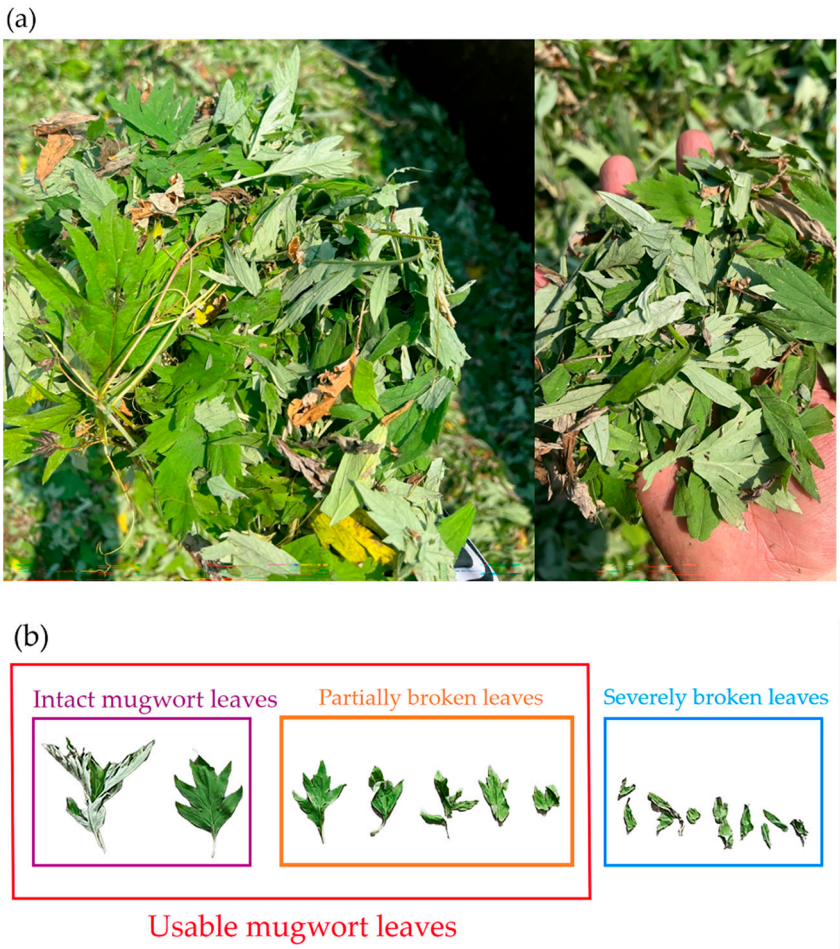

Figure 19. (**a**) Mugwort harvesting diagram; (**b**) leaf classification diagram.

Intact and partially broken leaves are classified as usable, whereas severely broken leaves are considered unqualified. The usability rate of mugwort leaves is calculated using the following formula:

$$P_s = \frac{m_p}{m_y} \times 100\% \tag{51}$$

$$P_k = (1 - P_s) \times 100\% \tag{52}$$

where P_s is the severe breakage rate of mugwort leaves in the bin, %; P_k is the usability rate of mugwort leaves in the bin, %; m_p is the mass of severely broken leaves in the bin, g.

5.3. Experimental Method

To determine the optimal working parameter combination for the harvester that achieves the highest net rate of mugwort leaf harvesting, the lowest impurity rate, and the highest mugwort leaf usability, a three-factor, five-level quadratic orthogonal rotating combination regression experiment was conducted, as shown in Table 5. The indicators—net rate of mugwort leaf harvesting, impurity rate, and mugwort leaf usability—are influenced by the forward speed, drum rotational speed, and cutting table height. Therefore, an orthogonal rotational combination design experiment was designed targeting these three factors.

Table 5. Experimental factor coding.

Code	Factors		
	Forward Speed (m/s)	Rotational Speed (r/min)	Height of Cutting Table (mm)
−1.628	0.4	160	40
−1	0.6	180	50
0	0.8	200	60
1	1.0	220	70
1.628	1.2	240	80

Based on preliminary experiments, it was found that when the forward speed exceeds 1.2 m/s and approaches 1.5 m/s, more mugwort leaves tend to remain on the stalks. This phenomenon indicates that at higher speeds, the contact time between the cutter and the stalks is too short, preventing effective leaf stripping. Consequently, this negatively impacts the harvesting performance and efficiency while increasing the burden of subsequent cleaning and processing. The minimum forward speed was set at 0.4 m/s to avoid a decline in harvesting efficiency caused by excessively low speeds. The drum rotational speed ranged from 160 to 240 r/min, and the cutting height varied between 40 and 80 mm. The coded levels for the experimental factors are listed in Table 6, with a total of 23 experimental combinations.

Table 6. Experimental program and results.

Experiment Number	Factors			S_j (%) Net Rate of Mugwort Leaf Harvesting	Z_z (%) Impurity Rate	P_k (%) Mugwort Leaf Usability Rate
	x_1	x_2	x_3			
1	0	0	0	93.89	12.02	84.49
2	0	−1.682	0	90.64	6.75	86.49
3	1	−1	1	89.87	9.87	86.78
4	1	1	1	95.02	15.63	86.32
5	0	0	0	94.82	14.42	86.15
6	0	0	0	94.17	13.62	84.63
7	1	−1	−1	90.19	9.14	87.64
8	−1	1	−1	98.14	16.31	81.67
9	0	0	0	93.42	11.83	85.57
10	0	0		94.64	12.67	85.47
11	−1	−1	1	93.65	9.18	84.61
12	1.682	0	0	91.12	11.36	87.33
13	0	0	1	93.38	11.92	84.75
14	0	0	−1.682	95.25	14.41	85.82
15	0	0	0	94.32	11.4	85.88
16	−1.682	0	0	95.21	10.64	84.56
17	0	0	0	94.47	12.89	84.53
18	−1	−1	−1	93.78	7.58	89.33
19	0	1	0	98.43	18.76	78.72
20	0	0	0	94.46	12.67	85.14
21	−1	1	1	96.25	14.23	81.14
22	0	0	0	95.36	11.17	85.35
23	1	1	−1	96.31	17.69	81.89

5.4. Analysis of Test Results

The net rate of mugwort leaf harvesting (S_j), impurity rate (Z_z), and mugwort leaf usability rate (P_k) were selected as the main evaluation indices. Each experimental group was repeated three times, and the average value was used as the final result. The test

results are presented in Table 6, where x_1, x_2, and x_3 represent the coded values of the experimental factors.

Data analysis was conducted based on the three-factor, five-level quadratic regression orthogonal rotary test design method. Regression analysis of the test results was performed using Design-Expert 13 software. The analysis of variance (ANOVA) of the regression models for the net rate of mugwort leaf harvesting, impurity rate, and mugwort leaf usability rate test results is shown in Table 7.

Table 7. Regression model ANOVA.

Source Variance	S_j Net Rate of Mugwort Leaf Harvesting				Z_z Impurity Rate				P_k Mugwort Leaf Usability Rate			
	Square Sum	Mean Square	*F*	*p*	Square Sum	Mean Square	*F*	*p*	Square Sum	Mean Square	*F*	*p*
Model	103.11	11.46	55.6	<0.0001 **	186.96	20.77	25.86	<0.0001 **	114.3	12.7	46.73	<0.0001 **
x_1	21.94	21.94	106.46	<0.0001 **	2.85	2.85	3.55	0.0821	8.13	8.13	29.92	0.0001 **
x_2	71.88	71.88	348.85	<0.0001 **	107.74	107.74	212.55	<0.0001 **	67.7	67.7	249.11	<0.0001 **
x_3	3.36	3.36	16.31	0.0014 **	2.63	2.63	3.28	0.0933	0.8865	0.8865	3.26	0.0941
x_1x_2	2.32	2.32	11.27	0.0052 **	0.0351	0.0351	0.0437	0.8376	3.03	3.03	11.13	0.0054 **
x_1x_3	0.021	0.021	0.102	0.7545	0.0903	0.0903	0.1124	0.7427	9.72	9.72	35.78	<0.0001 **
x_2x_3	0.9316	0.9316	4.52	0.0532	5.23	5.23	6.51	0.0241 *	11.23	11.23	41.33	<0.0001 **
${x_1}^2$	2.54	2.54	12.3	0.0039 **	4.05	4.05	5.04	0.0429 *	1.62	1.62	5.98	0.0295 *
${x_2}^2$	0.1146	0.1146	0.5561	0.4691	0.2134	0.2134	0.2656	0.6149	11.78	11.78	43.36	<0.0001 **
${x_3}^2$	0.0008	0.0008	0.0039	0.951	1.08	1.08	1.35	0.2669	0.1185	0.1185	0.4361	0.5205
Residuals	2.68	0.206			10.44	0.8033			3.53	0.2718		
Lack of Fit	0.235	0.047	0.1539	0.9729	1.64	0.3276	0.2977	0.9011	0.6732	0.1346	0.3766	0.8515
Error	2.44	0.3055			8.8	1.1			2.86	0.3575		
Total Sum	106.0				197.4				117.84			

Note: ** indicates highly significant ($p < 0.01$); * indicates significant ($0.01 \leq p \leq 0.05$).

(1) Net Rate of Mugwort Leaf Harvesting

From Table 7, it can be observed that among the main factors, the significance of the influence on the net rate of mugwort leaf harvesting (S_j) decreases in the following order: rotational speed (x_2), forward speed (x_1), and height of cutting table (x_3). The effect of rotational speed on the net rate of mugwort leaf harvesting was highly significant ($p < 0.01$), while the forward speed also had a significant impact. In contrast, the effect of cutting table height was relatively weak.

Regarding interaction effects, the interaction between forward speed and rotational speed (x_1, x_2) had a more significant impact on the net rate of mugwort leaf harvesting. Among the secondary main effect terms, the quadratic term of forward speed (${x_1}^2$) exhibited a highly significant effect on the net rate. Non-significant interaction terms and secondary main effect terms were combined into the residual term. After ANOVA, the regression equation describing the relationship between each factor and the net rate of mugwort leaf harvesting was obtained as follows:

$$S_j = 94.39 - 1.27x_1 + 2.29x_2 - 0.4961x_3 + 0.5388x_1x_2 - 0.3995{x_1}^2 \quad (53)$$

The above regression equation was tested for misfit, as shown in Table 7; the misfit term p = 0.9729, which is not significant ($p > 0.1$), and the test proved that there is a significant quadratic relationship between the indicator and the test factor.

(2) Impurity rate

As shown in Table 7, the experimental model was highly significant ($p < 0.01$). Among the main factors, the rotational speed (x_2) had the most significant effect on the impurity rate. The interaction of the rotational speed and the height of the cutting table (x_2, x_3) also significantly influenced the impurity rate. Regarding quadratic main effects, the quadratic term of forward speed (${x_1}^2$) had a significant impact on the impurity rate.

The sum of squares of the non-significant interaction terms and the quadratic main effect terms were incorporated into the residual term. Non-significant factors were excluded,

and ANOVA was performed to derive the regression equation for the factors and the impurity rate, as follows:

$$Zz = 12.52 + 0.457x_1 + 3.54x_2 - 0.4392x_3 - 0.8087x_2x_3 - 0.5046{x_1}^2 \quad (54)$$

The above regression equation was tested for misfit, as shown in Table 7. The misfit term p = 0.9011, which is not significant ($p > 0.1$), indicating that there is a significant quadratic relationship between the indicator and the test factors.

(3) Mugwort Leaf Usability

As shown in Table 7, the experimental model was highly significant ($p < 0.01$). Among the primary factors, forward speed (x_1) and rotational speed of the drum (x_2) exhibited highly significant effects. In terms of interaction effects, the interactions between forward speed and height of cutting table (x_1, x_3), rotational speed and height of cutting table (x_2, x_3), as well as forward speed and rotational speed (x_1, x_2) had highly significant impacts on the mugwort leaf usability. For the quadratic main effects, the quadratic term of rotational speed (${x_2}^2$) showed a highly significant effect on mugwort leaf usability, while the quadratic term of forward speed (${x_1}^2$) exhibited a significant effect.

The sum of squares of the non-significant interaction and quadratic main effect terms were incorporated into the residual term. Non-significant factors were eliminated, and ANOVA was performed to derive the regression equation for the factors and mugwort leaf usability, as follows:

$$P_k = 85.24 + 0.7717x_1 - 2.23x_2 - 0.2548x_3 + 0.615x_1x_2 + 1.1x_1x_3 + 1.19x_2x_3 + 0.3197{x_1}^2 - 0.8612{x_2}^2 \quad (55)$$

The regression equation above was subjected to misfit analysis, as shown in Table 7. The misfit term p = 0.8515, which is not significant ($p > 0.1$), indicating that the test confirms a significant quadratic relationship between the indicator and the test factors.

5.5. Response Surface Analysis

Using Design-Expert 13 software, the relationships between forward speed, rotational speed, and their combined effects on the net rate of mugwort leaf harvesting were analyzed, as shown in Figure 20a. The response surface plot shows that at a height of the cutting table of 60 mm, increasing the rotational speed improves the net rate of mugwort leaf harvesting. When the forward speed is constant, a higher rotational speed leads to a higher harvesting rate. Conversely, at a fixed rotational speed, an increase in forward speed reduces the rate. Notably, the harvesting rate drops sharply when the forward speed exceeds 0.9 m/s and the rotational speed is below 190 r/min. These results highlight the significant influence of rotational speed on the harvesting rate under a fixed cutting height and forward speed.

As shown in Figure 20b, the interaction between the height of the cutting table and the rotational speed also affects the impurity rate. At low rotational speeds, the cutting height has little impact on the net harvesting. However, at higher speeds, an increased cutting height reduces the efficiency due to decreased contact effectiveness. This indicates that while cutting height has an effect, rotational speed remains the dominant factor influencing the harvesting rate.

Field tests revealed that a lower height of the cutting table results in more impurities, such as withered leaves, during harvesting. Conversely, a higher cutting height reduces impurity inclusion. Uneven terrain in hilly areas often causes fluctuations in drum height, and a very low cutting height risks ground scraping, which can damage the tines and harm the mugwort root system. To address these issues, a hydraulic lifting mechanism was implemented for real-time adjustment of the cutting height. In the design, the height of the

cutting table was optimized at 40 mm to ensure efficient harvesting and operational safety for fresh mugwort leaf collection.

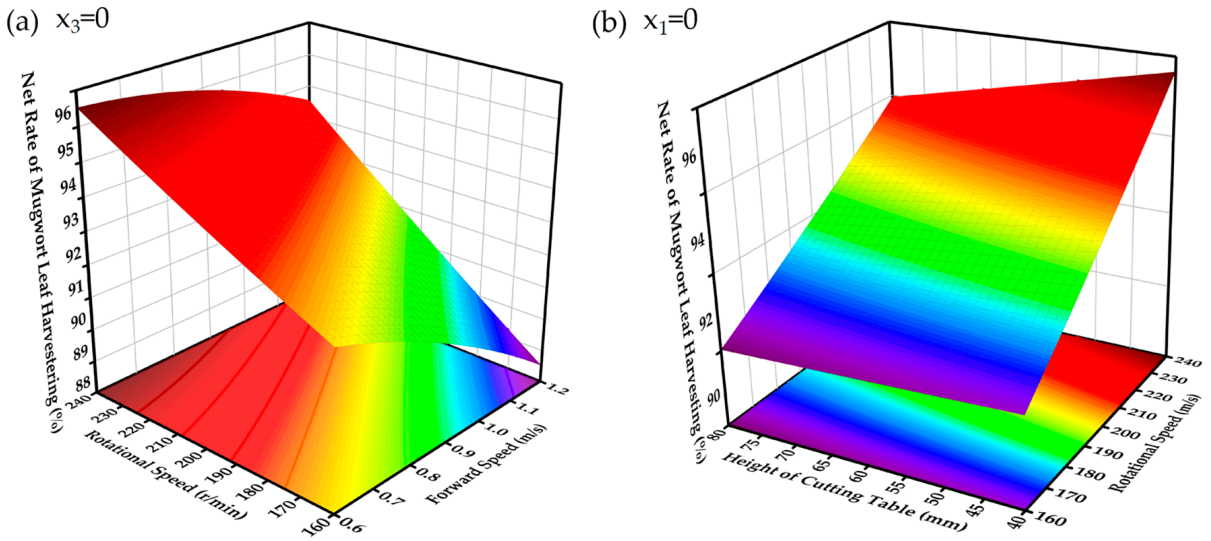

Figure 20. Response surface showing the effect of factor interactions on the net rate of mugwort leaf harvesting.

As shown in Figure 21a,b, Figure 21a illustrates the interaction between the height of cutting table and the rotational speed on the impurity rate, while Figure 21b depicts the interaction between forward speed and rotational speed on the impurity rate. Both figures indicate that the rotational speed is the primary factor affecting the impurity rate, whereas the forward speed has minimal influence.

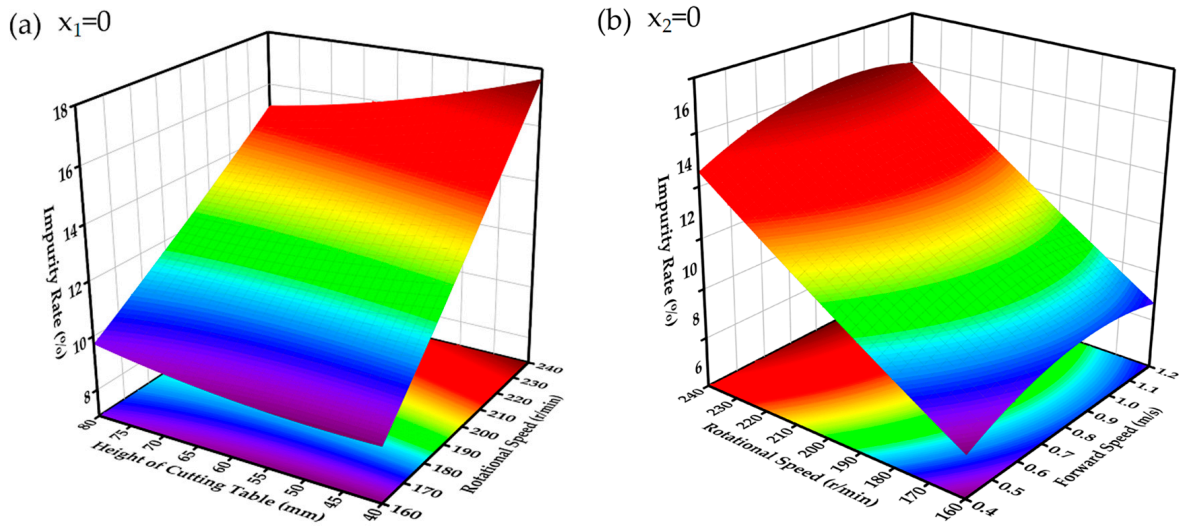

Figure 21. Response surface illustrating the effect of factor interactions on the impurity rate.

In Figure 21a, it is evident that higher rotational speeds combined with lower heights of cutting table lead to a higher impurity rate. This occurs because, at a constant forward speed, a lower cutting height and higher drum speed result in more frequent brushing of mugwort plants by the de-leafing tines. This increases the risk of breaking branches and collecting withered leaves from the plant base, thereby raising impurity levels.

To maintain a low impurity rate, the rotational speed must be carefully managed to avoid extremes, and the height of cutting table should be set at a moderate level. This

balanced approach ensures effective de-leafing while minimizing the inclusion of broken branches and withered leaves.

As shown in Figure 22a,b, the response surface plots illustrate the effects of various factor interactions on the mugwort leaf usability.

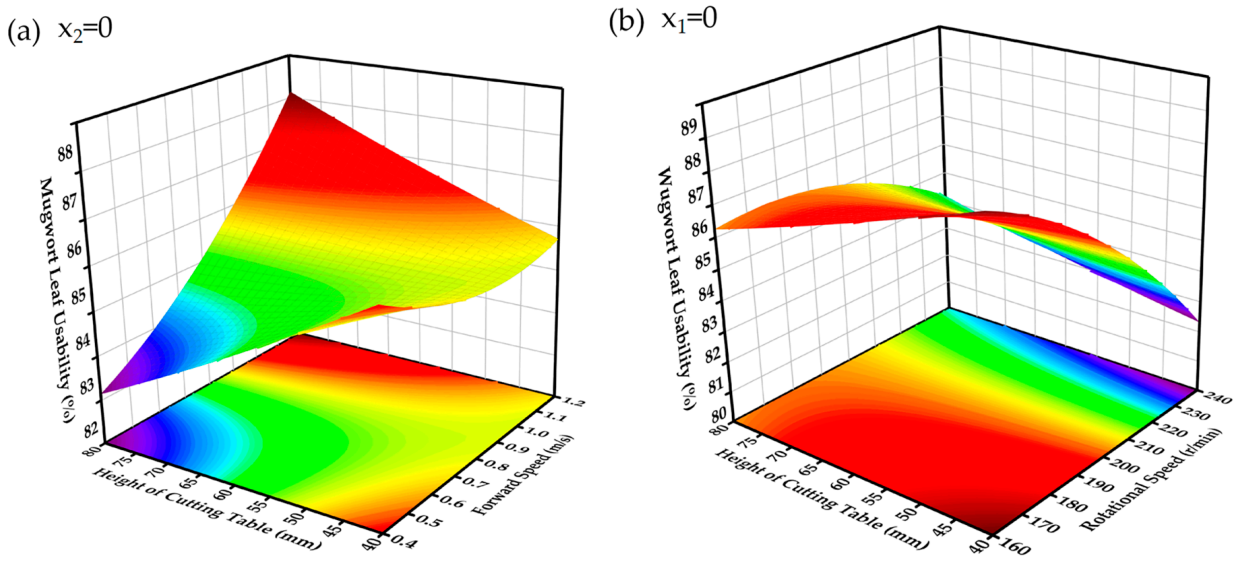

Figure 22. Response surface illustrating the effect of factor interactions on the usability rate of Artemisia leaves.

Figure 22a shows the interaction between forward speed and the height of the cutting table, revealing that both factors significantly affect leaf usability. The highest usability rate is achieved when the height of the cutting table is maintained within 45–55 mm and the forward speed is set between 0.7 and 0.9 m/s. However, when the cutting height is too low or too high, adjustments to the forward speed have minimal impact, indicating that the height of the cutting table plays a foundational role in determining overall usability.

Figure 22b illustrates the interaction between rotational speed and the height of the cutting table. The rotational speed has a significant impact on usability, with higher speeds leading to a sharp decline. This is due to the increased frequency of impacts from the de-leafing tines at higher speeds, causing greater damage to the mugwort leaves. The usability rate decreases markedly when the rotational speed exceeds 200–215 r/min.

To minimize damage and ensure a higher mugwort leaf usability, the rotational speed should be kept below 215 r/min. Additionally, maintaining the height of the cutting table between 45 and 55 mm and the forward speed within 0.7–0.9 m/s yields optimal results, maximizing usability while minimizing losses.

5.6. Parameter Optimization

To determine the optimal working parameters for the forward speed, rotational speed, and the height of the cutting table of the mugwort harvester, the optimization-numerical module in Design-Expert 13 software was utilized. The optimization process followed the principles of maximizing the net rate of mugwort leaf harvesting, minimizing the impurity rate, and enhancing the mugwort leaf usability. Based on the experimental conditions and

operational requirements of the harvester, the objective function and constraint conditions were defined as follows:

$$\begin{cases} \max S_j(x_1, x_2, x_3) \\ 6.55 \leq Z_z(x_1, x_2, x_3) \leq 18.36 \\ \max P_k(x_1, x_2, x_3) \\ s.t. \begin{cases} 0.7 \text{ m/s} \leq x_1 \leq 0.9 \text{ m/s} \\ 200 \text{ r/min} \leq x_2 \leq 215 \text{ r/min} \\ x_3 = 50 \text{ mm} \end{cases} \end{cases} \tag{56}$$

Considering the practical operational requirements of mugwort harvesting, the optimal parameter combination for the harvester was determined as follows: forward speed of 0.8 m/s, rotational speed of 200 r/min, and height of the cutting table of 50 mm. Under these conditions, the net rate of mugwort leaf harvesting was 94.64%, the impurity rate was 12.8%, and the mugwort leaf usability reached 85.39%.

5.7. Field Test

A field test was conducted in an Artemisia planting field in Qichun County, Hubei Province, to evaluate the performance of the mugwort harvester. The test site and results are shown in Figure 23a and 23b, respectively.

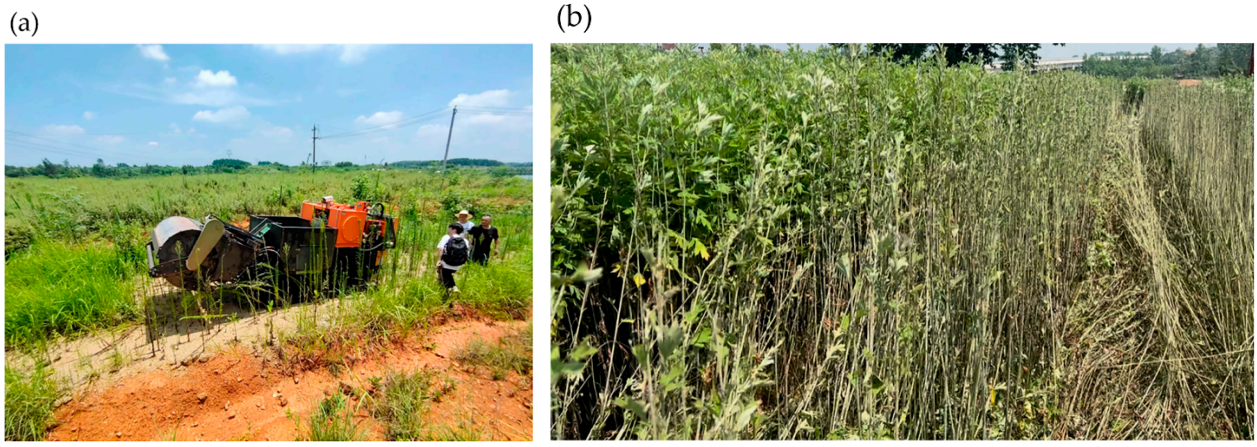

Figure 23. (**a**) Field test site. (**b**) Field test result.

The field test results were as follows: the harvesting efficiency reached 0.155 hm^2/h, with a net rate of mugwort leaf harvesting of 93.78%, an impurity rate of 13.96%, and a mugwort leaf usability of 86.23%, closely aligning with the optimal parameter combination predicted by the regression equation.

In summary, the mugwort harvester exhibited stable performance, characterized by a compact structure, ease of operation, high efficiency, and practical utility. These features make it highly suitable for integrated and mechanized mugwort harvesting operations in China, reducing labor requirements and enhancing operational efficiency.

6. Conclusions

(1) This study developed a self-propelled mugwort harvester specifically designed for hilly and mountainous terrains to address the challenges of manual harvesting. The harvester integrates a crawler-driven chassis, a tine drum de-leafing device, and a hydraulic system, with optimized technical parameters to enhance efficiency and performance. Mathematical models were established to evaluate the relationships between key operational parameters (rotational speed, forward speed, cutting table

height) and performance indicators (net harvesting rate, impurity rate, and mugwort leaf usability). Field tests validated the effectiveness of the harvester, achieving a net harvesting rate of 93.78%, an impurity rate of 13.96%, a usability rate of 86.23%, and an operational efficiency of 0.155 hm^2/h. These results highlight the harvester's ability to significantly reduce labor intensity and improve productivity, as manual harvesting achieves only 0.007 hm^2/h.

(2) The energy and cost analysis revealed that the harvester, powered by a diesel engine, consumes 15.6 L of fuel per hour under normal operating conditions. The primary cost factors include diesel consumption and maintenance expenses. These findings demonstrate the scalability and commercial viability of the harvester for large-scale operations.

(3) Despite its advantages, the current design has certain limitations. Manual unloading of the storage bin reduces overall efficiency, and the harvester only collects mugwort leaves, leaving stalks in the field. This necessitates additional equipment for field preparation to harvest mugwort stalks, which consequently increases labor intensity. Future designs should incorporate automated unloading systems and functionalities for stalk cutting or shredding to optimize workflow, reduce labor demands, and promote sustainable practices by returning organic material to the soil.

(4) The harvester provides significant economic and ecological benefits by improving operational efficiency, reducing labor costs, and enhancing the quality of harvested leaves to meet market demands. However, further research is needed to evaluate its adaptability to different terrains, environmental conditions, and various mugwort varieties. Additionally, future efforts should focus on improving the harvester's structure and expanding its functionalities to meet the evolving demands of large-scale mechanized mugwort harvesting, contributing to the sustainability and modernization of the industry.

Author Contributions: Conceptualization, Y.L., X.H. and Y.H.; investigation, Y.L., X.H. and Y.H.; writing—original draft preparation, Y.H. and K.Z.; writing—review and editing, Y.H., J.C., S.W. and Y.L.; supervision, Y.L.; project administration, Y.L. and X.H.; funding acquisition, Y.L. and X.H. All authors have read and agreed to the published version of the manuscript.

Funding: This research was funded by the Department of Agriculture and Rural Affairs of Hubei Province [grant number: HBSNYT202220] and the Key Research and Development Program of Hubei Province [grant number: 2022BBA0016].

Institutional Review Board Statement: Not applicable.

Data Availability Statement: The data presented in this study are available on request from the corresponding author.

Conflicts of Interest: The authors declare no conflicts of interest. The funders had no role in the design of the study; in the collection, analyses, or interpretation of data; in the writing of the manuscript; or in the decision to publish the results.

References

1. Zeb, S.; Ali, A.; Zaman, W.; Zeb, S.; Ali, S.; Ullah, F.; Shakoor, A. Pharmacology, taxonomy and phytochemistry of the genus artemisia specifically from pakistan: A comprehensive review. *Pharm. Biomed. Res.* **2018**, *4*, 1–12. [CrossRef]
2. Bisht, D.; Kumar, D.; Kumar, D.; Dua, K.; Chellappan, D.K. Phytochemistry and pharmacological activity of the genus artemisia. *Arch. Pharmacal Res.* **2021**, *44*, 439–474. [CrossRef]
3. Bora, K.S.; Sharma, A. The genus artemisia: A comprehensive review. *Pharm. Biol.* **2011**, *49*, 101–109. [CrossRef] [PubMed]
4. Siwan, D.; Nandave, D.; Nandave, M. Artemisia vulgaris linn: An updated review on its multiple biological activities. *Future J. Pharm. Sci.* **2022**, *8*, 47. [CrossRef]

5. Nigam, M.; Atanassova, M.; Mishra, A.P.; Pezzani, R.; Devkota, H.P.; Plygun, S.; Salehi, B.; Setzer, W.N.; Sharifi-Rad, J. Bioactive compounds and health benefits of artemisia species. *Nat. Prod. Commun.* **2019**, *14*, 1–17. [CrossRef]
6. Sun, Y.J.; Tian, J.J. Research on the application of big data in regional industrial supply chain. *J. Phys. Conf. Ser.* **2021**, *1883*, 012167.
7. Lai, Q.F.; Li, Y.R.; Yao, X.; Liu, B.; Deng, Y.J.; Hu, S.F.; Xiao, B.G. Research on shearing and beating hybrid mugwort deleafing mechanism. *Agric. Technol. Equip.* **2021**, 13–14+16.
8. Sun, S.N. An Experimental Study on the Influencing Factors of Defibration Quality of Artemisia Detachment. Master's Thesis, Hubei University of Technology, Wuhan, China, 2018.
9. Wang, D. Structural Design and Test Analysis of High-Efficiency Wormwood Defoliator. Master's Thesis, Hubei University of Technology, Wuhan, China, 2020.
10. Dong, W.T. Design and Experiment Research of *Artemisia argyi* Defoliation Machine. Master's Thesis, Huazhong Agricultural University, Wuhan, China, 2022.
11. Zhou, Y.; Huang, H.D.; Zhang, G.Z.; Fang, Z.; Xu, Z.J.; Wei, M. Design and experiment research of *Artemisia argyi* leaves removing machine. *Chin. Agric. Mech.* **2022**, *44*, 197–202.
12. Lu, E.; Xue, J.; Chen, T.; Jiang, S. Robust trajectory tracking control of an autonomous tractor-trailer considering model parameter uncertainties and disturbances. *Agriculture* **2023**, *13*, 869. [CrossRef]
13. Wang, T.B.; Wang, H.P.; Xiao, P.; Luan, Y.Q.; Li, L. Substation inspection robot crawler obstacle-navigation platform complex environment research. *Appl. Mech. Mater.* **2013**, *415*, 65–67. [CrossRef]
14. Wang, Z.; Kong, F.; Xie, Q.; Zhang, Y.; Sun, Y.; Wu, T.; Chen, C. Design and testing of a crawler chassis for brush-roller cotton harvesters. *Agriculture* **2024**, *14*, 1832. [CrossRef]
15. Yang, Z.Q. Crawler Vehicle Action System Dynamics Simulation and Fatigue Analysis. Master's Thesis, North University of China, Taiyuan, China, 2023.
16. Sun, Y.; Xu, L.; Jing, B.; Chai, X.; Li, Y. Development of a four-point adjustable lifting crawler chassis and experiments in a combine harvester. *Comput. Electron. Agric.* **2020**, *173*, 105416. [CrossRef]
17. Jiang, D. Dynamic simulation of crawler excavator walking mechanism. *Acta Tech.* **2017**, *62*, 255–264.
18. Fan, G.J.; Wang, Y.Z.; Zhang, X.H. Development and experiment of lifting platform for orchards in hilly area. *Appl. Mech. Mater.* **2017**, *865*, 111–117. [CrossRef]
19. Gupta, C.; Tewari, V.K.; Machavaram, R. Evaluation of a laboratory-based prototype of a comb-type picking mechanism for chili pepper harvester. *J. Biosyst. Eng.* **2022**, *47*, 69–78. [CrossRef]
20. Jameel, M.W.; Zaman, Q.U.; Schumann, A.W.; Quang, T.N.; Farooque, A.A.; Brewster, G.R.; Chattha, H.S. Effect of plant characteristics on picking efficiency of the wild blueberry harvester. *Appl. Eng. Agric.* **2016**, *32*, 589–598.
21. Farooque, A.A.; Zaman, Q.U.; Groulx, D.; Schumann, A.W.; Yarborough, D.E.; Nguyen-Quang, T. Effect of ground speed and header revolutions on the picking efficiency ofa commercial wild blueberry harvester. *Appl. Eng. Agric.* **2014**, *30*, 535–546.
22. Brabandt, H.; Ehlert, D. Chamomile harvesters: A review. *Ind. Crops Prod.* **2011**, *34*, 818–824. [CrossRef]
23. Ehlert, D.; Beier, K. Development of picking devices for chamomile harvesters. *J. Appl. Res. Med. Aromat. Plants* **2014**, *1*, 73–80. [CrossRef]
24. Han, D.; Zhang, H.; Li, G.; Wang, G.; Wang, X.; Chen, Y.; Chen, X.; Wen, X.; Yang, Q.; Zhao, R. Development of a bionic picking device for high harvest and low loss rate pod pepper harvesting and related working parameter optimization details. *Agriculture* **2024**, *14*, 859. [CrossRef]
25. Yang, J.; Qin, X.; Lei, J.; Lu, L.; Zhang, J.; Wang, Z. Design and experiment of a crawler-type harvester for red cluster peppers in hilly and mountainous regions. *Agriculture* **2024**, *14*, 1742. [CrossRef]
26. Liu, Z.Y.; Jin, C.Q.; Yuan, W.S.; Feng, Y.K.; Yuan, J.M. Design optimization and experiment of spring-tooth drum type picking device for vegetable soybean harvester. *Trans. Chin. Soc. Agric. Eng.* **2022**, *53*, 171–180.
27. Qu, Z.; Lu, Q.; Shao, H.; Liu, L.; Wang, X.; Lv, Z. Design and testing of a self-propelled dandelion seed harvester. *Agriculture* **2023**, *13*, 917. [CrossRef]
28. Ling, J.; Shen, H.; Gu, M.; Hu, Z.; Zhao, S.; Wu, F.; Xu, H.; Gu, F.; Zhang, P. The design and optimization of a peanut-picking system for a fresh-peanut-picking crawler combine harvester. *Agriculture* **2024**, *14*, 1332. [CrossRef]
29. Li, L.; Li, S.; Li, J.; Wen, B.; Cen, H.; Wang, M.; Li, Y.; Song, K.; Zhang, Z. Design and test of a comb-brush-type honeysuckle-picking device. *Agriculture* **2023**, *13*, 2088. [CrossRef]
30. Wang, L.; Liu, F.; Wang, Q.; Zhou, J.; Fan, X.; Li, J.; Zhao, X.; Xie, S. Design of a spring-finger potato picker and an experimental study of its picking performance. *Agriculture* **2023**, *13*, 945. [CrossRef]
31. Breidi, F.; Garrity, J.; Lumkes, J. Design and testing of novel hydraulic pump/motors to improve the efficiency of agricultural equipment. *Trans. ASABE* **2017**, *60*, 1809–1817. [CrossRef]
32. Wang, S.; Zhang, D.; Hu, X.; Lu, R. Finite element simulations and experimental analysis for efficient mugwort harvesting. *Agriculture* **2024**, *14*, 1875. [CrossRef]

33. Rizaev, A.; Matchanov, R.; Yuldashev, A.T.; Kuldashev, D.A.; Djuraeva, N.B.; Karimov, N.; Ashurov, N. Cotton harvesters for one-time cotton-picking. *IOP Conf. Ser. Mater. Sci. Eng.* **2021**, *1030*, 012173. [CrossRef]
34. Mei, F.W.; Zhang, Z.Y.; Li, X.D.; Zhao, W.; Cao, H.; Zhu, X.H. Spring-tooth type unbaling anti-blocking device for orchard straw mulching machine. *Trans. CSAE* **2023**, *39*, 25–34.
35. Du, D.D.; Fei, G.Q.; Wang, J.; Huang, J.J.; You, X.R. Development and experiment of self-propelled cabbage harvester. *Trans. CSAE* **2015**, *31*, 16–23.
36. Zhang, Z.G.; Wang, Y.C.; Li, H.Q.; Dao, F.; Zhang, Z.D.; Xue, H.T. Design and test of hydraulic control tracked self-propelled greenhouse panax notoginseng harvester. *Trans. Chin. Soc. Agric. Eng.* **2021**, *52*, 127–135+158.
37. Wang, B.S.; Wang, W.Z.; Wang, M.S.; Zhong, D.F.; Chen, J. Design and experiment of full hydraulic drive high clearance tracked vehicle. *Trans. Chin. Soc. Agric. Eng.* **2016**, *47*, 471–476.
38. Shin, S.Y.; Kim, M.H.; Cho, Y.; Kim, D.C. Performance testing and evaluation of drum-type stem-separation device for pepper harvester. *Appl. Sci.* **2021**, *11*, 9225. [CrossRef]
39. Kim, T.H.; Kim, D.C.; Cho, Y. Performance comparison and evaluation of two small chili pepper harvester prototypes that attach to walking cultivators. *Appl. Sci.* **2020**, *10*, 2570. [CrossRef]
40. Chen, Y.; Wang, G.; Wang, J.; Zhang, P.; Wang, B.; Hu, Z. Adaptabilities of different harvesters to peanut plants after cutting stalks. *Int. J. Agric. Biol. Eng.* **2022**, *15*, 93–101. [CrossRef]